Damage Detection using SONIC IR Imaging for Composite Laminate

by

Aryabhat Darnal

A Thesis Presented in Partial Fulfillment
of the Requirements for the Degree
Master of Science

Approved July 2019 by the
Graduate Supervisory Committee:

Yongming Liu, Chair
Houlong Zhuang
Qiong Nian

ARIZONA STATE UNIVERSITY

August 2019

ABSTRACT

Non-Destructive Testing (NDT) is a branch of scientific methods and techniques used to evaluate the defects and irregularities in engineering materials. These methods conduct testing without destroying or altering material's structure and functionality. Most of these defects are subsurface making them difficult to detect and access.

SONIC INFRARED (IR) is a relatively new and emerging vibrothermography method under the category of NDT methods. This is a fast NDT inspection method that uses an ultrasonic generator to pass an ultrasonic pulse through the test specimen which results in a temperature variation in the test specimen. The temperature increase around the area of the defect is more because of frictional heating due to the vibration of the specimen. This temperature variation can be observed using a thermal camera.

In this research study, the temperature variation in the composite laminate during the SONIC IR experimentation using an infrared thermal camera. These recorded data are used to determine the location, dimension and depth of defects through SONIC IR NDT method using existing defect detection algorithms. Probability of detection analysis is used to determine the probability of detection under specific experimental conditions for two different types of composite laminates. Lastly, the effect of the process parameters such as number of pulses, pulse duration and time delay between pulses of this technique on the detectability and probability of detection is studied in detail.

ACKNOWLEDGMENTS

I would like to express my deepest appreciation to my supervisor, Dr. Yongming Liu who provided me the opportunity to work under his guidance and mentorship towards my master's thesis. I really appreciate all the time, help and effort, which he has invested in me and my research. Especially, I would like to acknowledge his guidance and support throughout these two years both in academic and non-academic situations. Special thanks to Dr. Qinan Chang for her explicit support and guidance which helped me understand this research.

I gratefully acknowledge School for Engineering of Matter, Transport & Energy, Arizona State University for their support in my research study.

TABLE OF CONTENTS

Page

LIST OF TABLES

Table Page

LIST OF FIGURES

Figure Page

Figure Page

Figure Page

Figure Page

CHAPTER 1

INTRODUCTION

Mechanical equipment and components under various kinds of loads and damages during its life of operation. Most these damages and defects are subsurface (below the surface) and cannot be detected easily. There are inspection techniques which can be used to evaluate these components effectively. These inspection techniques come under the class of Nondestructive Testing (NDT) techniques. These methods not only locate defects in the component and but also their shape, size, depth etc.

In our research, we analyze a nondestructive inspection method known as SONIC Infrared (IR) testing NDE method. SONIC IR comes under the category of 'vibrothermography' which is a non-destructive inspection method which analyses the heat produced by the damages in a component when an ultrasonic signal is applied to it.

SONIC IR is an inspection technique that uses a short high frequency pulse which is applied at a convenient point on the surface of the component under study. The pulse typically ranges from 50 to 300ms and the frequency is of the range 20 to 40 KHz [1]. The pulse signal produces localized frictional heating near the defect area. The frictional heating is caused because the two surfaces of internal defects do not vibrate in unison when sound propagates through the component. Due to this frictional heating, the temperature near the defect area rises as compared to the other areas and this serves as the basis of this non-destructive method. The temperature rise is observed through an IR camera. The defects appear as bright spots against a dark background when seen through the IR camera.

1.1

LITERATURE REVIEW

SONIC IR method comes under the classification of Infrared thermography (IRT) nondestructive testing techniques. Infrared thermography is an accurate and quick nondestructive testing method widely used for inspection of mechanical components. Mechanical components undergo severe damages during their operation cycle which causes defects in the components. Most of these defects occur at subsurface levels of the components which are difficult to detect. IRT can be categorized into two categories: passive(stationary) and active(non-stationary) thermography [1].

Active thermography involves using external excitation source like optical radiation(laser), electromagnetic stimulation (induced eddy current), ultrasonic waves to generate heat around the damage/defect area in the component resulting in a temperature increase which can be recorded with an IR camera [1]. Some of the active IRT methods for defect detection are reviewed and discussed in the next section.

Optically Stimulated Thermography

An optical heat source is used to generate thermal waves in this category of thermography. The most commonly used methods are Pulsed thermography (PT), Lock-in thermography (LIT), Step heating thermography (SHT), Long pulse thermography (LPT) etc. [1]. Some of these are discussed below:

1. Pulsed Thermography

   Pulsed Thermography (PT) uses a high intensity pulse of light to heat the surface of the test component via photothermal effect [1]. The duration of light pulse ranges from 0.1 to 50ms depending on the thermal properties of the component and the defect depth [1]. The temperature T at a depth d at a time t after a uniform impulse of energy Q is given by [1]:

$$T = \frac{Q}{2\zeta\sqrt{\pi t}} e^{\frac{-d^2}{4\alpha t}} \quad (1)$$

   ζ = Thermal effusivity of the material (W $s^{1/2}$ m^{-2} K^{-1})

   α = Thermal diffusivity of the material (m^2/s)

2. Lock-in Thermography (LIT)

   An external periodic heat excitation is used to generate thermal waves in the test specimen [1]. The LIT method is less sensitive to the local variations of surface emissivity [1].

   For a homogenous isotropic semi-infinite material with the surface being uniformly illuminated by a periodically modulated light beam with intensity q_d, the temperature T at a depth d is given by [1]:

$$T = \frac{Q}{2\zeta\sqrt{\omega}} e^{\frac{-d}{\mu}} e^{j(\omega t - \frac{d}{\mu})} \quad (2)$$

$$q_d = \frac{Q[1 + \exp(j\omega t)]}{2} \quad (3)$$

ω = Angular modulation of the heat source

μ = Thermal diffusion length of the material

ζ = Thermal effusivity of the material (W $s^{1/2}$ m^{-2} K^{-1})

3. Step Heating and Long Pulse Thermography (SHT and LPT)

In both SHT and LPT, a low intensity step-pulse heat source is applied for a long period of time typically ranging from milliseconds to few seconds, which enables a longer heating time to detect deeper defects in the test specimen [1]. In SHT, the data is recorded during the experimentation whereas in LPT the data is acquired during the cooling phase. The temperature T at the surface of the test specimen of depth D is given by [1]:

$$T = \frac{2Q}{\zeta}\sqrt{\frac{t}{\pi}}\left[1 + \sqrt{\pi}\sum_{n=1}^{\infty} 2\text{ierfc}\left(\frac{nD}{\sqrt{\alpha t}}\right)\right] \tag{4}$$

$$\text{ierfc}(x) = \frac{1}{\sqrt{\pi}\exp(-x^2) - x.\,\text{erfc}(x)} \tag{5}$$

Ultrasonic Stimulated Thermography

One of the shortcomings of optically stimulated thermography is its inefficiency in detecting in-depth defects and damages. Using external optical heat sources limits the detection of defects located beneath the surface of the test specimen.

Ultrasonic stimulated thermography involves generating powerful vibrations of short time period in the test specimen causing frictional heating around the defects. The resulting temperature change on the surface of the specimen around the defect is detected using an infrared camera. Vibrations are produced in the test specimen using an ultrasonic transducer that is in contact with the surface of the component under testing. The frequency ranges from 15-50 kHz [1] and the duration of the pulse varies from 30 – 200ms [1].

Xiaoyan Han *et al.* [2] reviewed the application of SONIC IR imaging for disbonds and delaminations in composites and use of broadband chaotic sound to eliminate artefacts resulting from acoustic interference. SONIC IR method has the capability of detecting tight disbonds that are usually not detectable using conventional thermography methods. The use of chaotic sound eliminates the acoustic mode patterns and interferences due to the heating of the specimen.

X. Han *et al.* [3] studied the effect of structure and relative position of the sound source on the defects in SONIC IR testing method. From the study, it was observed that the acoustic behavior of composites is different from that of metals. The detectability of defects depends on the composite structure and relative locations between the ultrasound source and the defects. Due to attenuation of sound propagation in composites, time duration for the ultrasonic pulse signal is longer as compared to that for metal structures. Through this study, it was shown that SONIC IR imaging can be used for fast wide area inspection in composite structure and detect disbond in aircraft composite.

Eddy Current Stimulated Thermography

Eddy Current Stimulated Thermography (ECST) involves inducing eddy currents in a conductive material through a coil and the temperature due to induction heating is observed with an IR camera [1]. When eddy currents encounter a damage/defect in the material, it diverts and changes the direction of the current flow. This results in areas of increased and decreased eddy current density leading to relatively hot and cool areas [1]. High eddy

current pulse with frequency ranging from 150-450 kHz [1] is applied for period ranging from few milliseconds for high-conductivity materials like metals to few seconds for low-conductivity specimens like plastics and carbon fiber reinforced plastic laminates.

Defect Detection

The main objective of this research is to detect defect in composite laminates through the SONIC IR NDT method. The research objectives include using existing algorithms for image processing and analysis models, analytical model for defect depth determination, determining the reliability of the SONIC IR method through the POD model and analyzing the process parameters of the experiment.

Defect detection in thermal images is used to evaluate the effectiveness of an NDT method to detect the defects present in the component under study. Several research works have been conducted for the object detection in images.

The algorithms for defect detection can be categorized into two categories namely nondedicated and dedicated algorithm. A nondedicated algorithm is not specifically used for thermal images while a dedicated algorithm is specifically used for thermal images.

Thresholding is the most common method for object separation in images owing to its simplicity [4]. Most commonly the histogram of the image in thresholding method. If an image f(x,y) where f is the gray level of each pixel of the image is composed of a bright object on a dark background, a threshold T is determined from the gray level histogram of the image which separate the bright object from the dark background.

A thresholded image h(x,y) from an image f(x,y) can be defined as [4]:

$$h(x,y) = 1 \text{ if } f(x,y) > T$$

$$h(x,y) = 0 \text{ if } f(x,y) \leq T$$

If the gray-level histogram is determined for the entire image, then the threshold T is the global threshold level whereas if the threshold level is derived from an area of the image then it is referred as local threshold level [4].

Mehmet Sezgin and Bulent Sankur [5] categorized thresholding techniques into six types:

1. Histogram shape-based thresholding method
2. Clustering based thresholding method
3. Entropy based thresholding method
4. Object-attributed based method
5. Spatial methods
6. Local methods

Otsu [6] proposed a thresholding method in which the threshold is selected by maximizing the between-class variances. Otsu presented a nonparametric and unsupervised method of automatic thresholding of images for image segmentation. This method is used to automatically select a threshold from a grey level histogram of the image using the discriminant analysis. The optimal threshold is determined by maximizing the discriminant measure or the measure of separability of the resultant classes in gray levels of the image.

Rosenfield and DelaTorre [7] proposed segmentation of image into gray level subpopulations is by selecting thresholds at the bottoms of valleys on the histogram. If the subpopulations overlap, valleys may not exist, but it is still possible to select thresholds at the shoulders of the histogram peaks. Both valleys and shoulders correspond to concavities on the histogram and the deepest concavity point becomes the candidate for selecting the thresholds.

Kapur *et al.* [8] proposed an algorithm for selecting a threshold from the gray level histogram of an image using the entropy concept from information theory. In this algorithm, the foreground and background of the image are considered two different signal sources and when the sum of the two class entropies reaches it maximum, the optimum threshold is obtained.

Tsai [9] used moment preserving principle for optimal threshold selection. Before thresholding the image, the gray level moments of the image are determined. The thresholds are then selected in such a way that the moments of the thresholded image are preserved.

Niblack's binarization method (NBM) is one of the oldest local binarization method [10]. In this method, the threshold value is determined by calculating the local mean and standard

deviation of pixels value in a local window of an image. The threshold formula used is defined as [10]:

$$T_d = u(x,y) + k * s(x,y) \tag{6}$$

where u (x, y) and s (x, y) are the local mean and standard deviation and k is an image dependent manually selected parameter (−0.2 for dark foreground and 0.2 for dark background).

Due to the limitations of the non-dedicated algorithms for defect detection in thermal images, dedicated algorithms have been proposed and developed.

Hamadani [4] used first-order statistics properties, mean, u, and standard deviation, s, to extract a bright object in a thermal image. The threshold level of an image of size M x N is given by [4]:

$$T = k_1 * u + k_2 * s \tag{7}$$

$$u = \frac{1}{M * N} \sum_{i=1}^{M} \sum_{j=1}^{N} f(i,j) \tag{8}$$

$$s = \sqrt{\frac{1}{M * N} \sum_{i=1}^{M} \sum_{j=1}^{N} (f(i,j) - u)^2} \tag{9}$$

Sapina [11] method includes using six textural features of an image based on the gray level co-occurrence matrices (GLCM) to segment the warm objects from the background of the image. The six textural features used are: maximum probability, uniformity of energy, inverse difference moment, contrast, variance and correlation. After obtaining the textural features images, further image processing is required to clearly separate the defects from the background.

X. Maldague *et al.* [12] proposed an algorithm for defect extraction in infrared or low spatial content images. First, the potential defect locations are determined by spatial sorting of the pixels in decreasing order of their brightness. Pixel labeling is performed on the basis of the distance. The shape of the defect is obtained by gradually decreasing the threshold until it encounters a sudden increase in the number of pixels agglomerates, or an image boundary is encountered.

Depth Estimation

Many depth estimation methods have been proposed for determining the depth of the defect in the test specimen for the pulsed thermography NDE method. These methods involve using a specific characteristic time from the temperature decay curve and it is correlated to the depth of the defect. Some of the examples of these methods are peak contrast method, peak slope method, half rise method, half rise contrast method, early time method, absolute peak slope method, deviation time method, logarithmic first derivative half rise method and logarithmic peak second derivative time method.

For pulsed thermography, the temperature decay around the defect area as a function of time is defined as [14]:

$$T(t) = \frac{Q}{\rho C L}\left[1 + 2\sum_{n=1}^{\infty} \exp\left(-\frac{n^2\pi^2}{L^2}\alpha t\right)\right] \tag{10}$$

Q = Input energy per unit area (J/m^2)

ρ = Density (kg/m^3)

C = Specific heat (J/kgK)

α = Thermal diffusivity (m^2/s)

L = Sample thickness (m)

The temperature contrast (ΔT) is defined as the difference between the temperature around the defect area (T) and temperature of the reference area of the test specimen (T_r).

$$\Delta T = T - T_r$$

1. Peak Temperature Contrast Method

The temperature contrast is defined as [14]:

$$\Delta T = T - T_r$$

$$\Delta T = \frac{Q}{\rho C L}\left[1 + 2\sum_{n=1}^{\infty}\exp(-n^2\omega)\right] - \frac{Q}{\rho C L_r}\left[1 + 2\sum_{n=1}^{\infty}\exp(-n^2\omega_r)\right] \quad (11)$$

$$\omega = \frac{\pi^2 \alpha t}{L^2}\ ;\ \omega_r = \frac{\pi^2 \alpha t}{L_r^2} \quad (12)$$

Due to 3D heat conduction effect, the temperature contrast first increases and then decreases with respect to time [14]. The time at which the thermal contrast reaches its maximum value is defined as the characteristic time. It was observed that this characteristic time is approximately proportional to the square of the defect depth.

2. Peak Temperature Contrast Slope Method

In this method, the characteristic time is defined as the time at which the first derivative of the temperature contrast reaches its peak value. The temperature contrast slope can be defined as [14]:

$$\Delta T = \frac{Q}{\rho C L}\left[1 + 2\sum_{n=1}^{\infty}\exp(-n^2\omega)\right] - \frac{Q}{\rho C L_r}\left[1 + 2\sum_{n=1}^{\infty}\exp(-n^2\omega_r)\right]$$

(13)

Substituting

$$z = \frac{L}{L_r}$$

(14)

$$V = \frac{T C L_r \rho}{Q}$$

(15)

$$\Delta V = \frac{1}{z} - 1 + 2\sum_{n=1}^{\infty}\frac{e^{-\frac{n^2\omega_r}{z^2}}}{z} - e^{-n^2\omega_r}$$

(16)

$$\frac{d(\Delta V)}{d\omega_r} = \sum_{n=1}^{\infty} 2n^2\left(e^{-n^2\omega_r} - \frac{e^{-\frac{n^2\omega_r}{z^2}}}{z^3}\right)$$

(17)

The peak slope time T_s is approximately proportional to the defect depth and the proportionality constant does not depend on the defect size. T_s can calculated by equating the second derivative of equation (17) to 0.

$$T_s = \frac{3.64L^2}{\pi^2\alpha}$$

(18)

3. Logarithmic Peak Second Derivative Method

In Logarithmic Peak Second Derivative Method, the peak of the second derivative of the surface temperature of the specimen on a logarithmic scale is used to estimate the defect depth. The surface temperature of the test specimen is given by [14]:

$$T(t) = \frac{Q}{\rho CL}\left[1 + 2\sum_{n=1}^{\infty} \exp\left(-\frac{n^2\pi^2}{L^2}\alpha t\right)\right] \tag{19}$$

The first derivative of the surface measured temperature is calculated as [14]:

$$\frac{d(\ln T)}{d(\ln t)} = \frac{t}{T}\frac{dT}{dt} \tag{20}$$

The second derivative is calculated as [14]:

$$\frac{d^2(\ln T)}{d(\ln t)^2} = \frac{t}{T}\frac{dT}{dt} - \frac{t^2}{T^2}\left(\frac{dT}{dt}\right)^2 + \frac{t^2}{T}\frac{d^2T}{dt^2} \tag{21}$$

$$\frac{dT}{dt} = -\frac{Q}{\rho CL}\frac{2\omega}{T}\sum_{n=1}^{\infty} n^2 e^{-n^2\omega} \tag{22}$$

$$\frac{d^2T}{dt^2} = \frac{Q}{\rho CL}\frac{2\omega^2}{T^2}\sum_{n=1}^{\infty} n^4 e^{-n^2\omega} \tag{23}$$

Solving the above two equations, the second derivative peak time T_P obtained is given by:

$$T_P = \frac{L^2}{\pi\alpha} \tag{24}$$

4. Least Squares Fitting Method

J.G. Sun [15] proposed a theoretical heat transfer model for fitting the temporal data at each of the surface point. For the time between $0<t<t_b$, the temperature T is given by [15]:

$$T(t) \approx A\left[1 + 2\sum_{n=1}^{\infty} \exp\left(-\frac{n^2\pi^2}{L^2}\alpha t\right)\right] - st \tag{25}$$

The slope s is determined by linear fitting of the experimental data in the time $t_a<t<t_b$. The time t_a and t_b are calculated as [15]:

$$t_a = \frac{L^2}{2\alpha}\ ;\ t_b = 3t_a \tag{26}$$

Omar Obeidat *et al.* [16] developed a model that described the heat diffusion from the subsurface defect in a composite material using Green's function procedure. The model is used to map some characteristic time quantities from the temperature time curve with the defect depth. The time quantities used are half-maximum power time, peak slope time and second derivative peak time.

Probability of Detection

Probability of Detection (POD) is the study of reliability of an NDE method for detecting the defects present in a test specimen.

Jun-zhen Zhu *et al.* [17] tested a set C45 ferritic steel plates with artificial fatigue cracks. The crack heating response increased with the increasing crack length and a linear relationship between the logarithmic form of heat response signal and the crack length was observed. Linear regression analysis and Wald method is used to estimate the POD function and its confidence bounds. The test provided a quantitative evaluation of the detection reliability in sonic infrared imaging.

N Yusa [18] proposed a POD model to study the efficiency of NDE testing methods for detection of stress corrosion cracks appearing in the steam generator tubes of pressurized water reactors. Three-dimensional finite element simulations were conducted to determine eddy current signals due to stress corrosion cracks. The probabilistic nature of the NDE test is simulated by varying the electrical conductivity of the modelled stress corrosion cracking. A two-dimensional POD model is proposed which expresses the POD as a function of the depth and length of a crack.

Vamsi Krishna Rentala *et al.* [20] proposed a model-based approach for evaluating the POD. The POD depends on factors such as material properties, geometry of the specimen, defect features, testing methods etc. Due to the number of factors affecting the POD, Model Assisted Probability of Detection (MAPOD) curves is used. In this research, MAPOD approach was studied with respect to selecting crack sizes distribution, censoring and

regression, estimation of distribution parameters. A COMSOL Multiphysics based FEM numerical model is developed to simulate ultrasonic response from a Ti-6Al-4V cylindrical block and validated experimentally. Individual ultrasonic response from various flat bottom hole defects was also generated using numerical model. Using the POD curve, the flaw size corresponding to 90% probability and 95% confidence is obtained. Also, it is observed that the POD value increased with an increase in decision threshold value.

J. DiMambro *et al.* [21] of Sandia National Laboratories, Airworthiness Assurance, Albuquerque implemented two crack POD experiments to compare the reliability of SONIC IR Imaging and Fluorescent Penetrant Inspection (FPI) methods. Blind SONIC IR and FPI inspections are performed on titanium and Inconel specimens having statistically relevant flaw profiles. SONIC IR achieved higher POD for fatigue crack length of 0.04" and more. Cracks less than 0.04" are more likely to be detected by FPI but there is a high chance of false call rate. This indicates that FPI is not designed for detecting deep cracks and it is also responsive to other surface conditions (porosity, machine marks etc.). SONIC IR POD is dependent on the flaw size while it does not depend on flaw size in case of FPI. Also, the SONIC IR inspection does not affect the crack length.

1.2

OBJECTIVE AND MOTIVATION

Composite materials are widely used in automotive, energy, transportation and aerospace applications. Fiber-reinforced composites are used as the primary structural material in most of the applications. Although composite materials provide excellent strength to weight ratio and material performance, some internal defects like inclusions, porosity, delaminations may be present due to the production process. These defects and delaminations results in the reduction of material strength and reliability of the composite structure which leads to eventual failure.

As these composite structures are expensive to manufacture, destructive technique is not economical to determine its reliability. The commonly used nondestructive testing methods used include pulsed thermography, magnetic particle testing, liquid penetrant testing, eddy current thermography, acoustic emission testing etc. SONIC IR testing comes under the classification of ultrasonic testing.

SONIC IR testing is a relatively new technique that can detect flaws that are difficult to detect with other methods such as tightly closed cracks. It has a quick and simple methodology requiring less time for setup and testing as compared to other conventional methods. Not many studies have been conducted on this defect detecting method regarding its affordability, reliability and efficiency in detecting subsurface defects. SONIC IR has a lot of potential as a new nondestructive technique and studying it forms the primary motivation of this research work.

The objective of this study is to determine the accuracy of this method in detecting subsurface defect delaminations in aircraft grade composite laminates and comparing it with the ground truth. To determine the reliability of this method, the Probability of Detection of this method is analyzed taking in account the defect characteristics. And to find the effect of the process parameters on the output, detailed process parameter study is conducted.

1.3

PROPOSED TASKS

In this section, proposed tasks to be performed as a part of this research project are discussed. These tasks are discussed in detail in the different chapters of this research.

1. Perform the experimentation and record the data (video) using the thermal infrared camera and the software packages. Export the data(video) as multiple images for image processing and analysis. Obtain the temperature data of the region of interest i.e. the defect area during the experimentation using the ResearchIR software package.
2. The infrared thermal images obtained from the experimentation is used for thermal image analysis and processing. Both non-dedicated and dedicated algorithms are used for detecting the defect delaminations and compared to the ground truth.
3. Use the temperature history of the composite laminate and the defect areas for determining the Probability of Detection (POD) of the NDT method. The POD analysis helps determining the reliability of the NDT method to detect defects with respect to some important parameters of the defects.
4. The temperature-time curve will be used for the analytical study of determining the relationship between the defect depth and various time quantities.
5. Determine the parameters of the experiment and study their effect on the defect detection accuracy and probability of detection.

CHAPTER 2

DESIGN OF EXPERIMENT

The equipment and components are used for the experimental setup are described below:

1. Infrared Thermal Camera

   The thermal camera is used to detect and capture the temperature change on the surface of the composite laminate during the experimentation. The camera used for the study is the **HIGH-RESOLUTION SCIENCE GRADE FLIR A655sc**.Below are the specifications of the IR camera:

Resolution	640 x 480
Detector Type	Uncooled Microbolometer
Dynamic Range	16-bit
Power	12/24 VDC, 24 W Absolute Max.
Spectral Range	7.5 – 14.0 µm
Operating Temperature Range	-15°C to 50°C (5°F to 122°F)
Optional Temperature Range	Up to 2,000°C (3,632°F)
Standard Temperature Range	(–40°C to 150°C) & (100°C to 650°C)
Frame Rate [Full Window]	50 Hz
Accuracy	±2°C or ±2% of Reading
NETD	<30 mK

Table 1: IR camera specifications

Figure 1: Infrared Thermal Camera

2. Ultrasonic Transducer

   A transducer is a device which converts one form of energy to another. In SONIC IR NDE, the transducer converts the electric pulse from the DC supply into sound waves that penetrate and travel through the composite laminate. This transducer comes under the classification of contact transducer as the transducer is used in direct contact with the test specimen.

Figure 2: Ultrasonic Transducer

3. Multiplexer

The multiplexer (MUX) is a combinational logic circuit designed to switch one of several input lines through to a single common output line. They operate like fast acting multiple position rotary switches controlling multiple channels one at a time to the output.

For this experiment, USB controlled IA-3133-U2i multiplexer is used. It is a 32-relay multiplexer.

Figure 3: Multiplexer

Aluminum extrusions, joints, nuts, BNC cables, wire strippers, tapes and other hardware tools are also required for connecting these components.

Software packages are used to control these devices and components during the experimentation. The software packages are listed below:

1. LABVIEW

   Laboratory Virtual Instrument Engineering Workbench (LabVIEW) is used to design the circuit and the user control panel through which the user can control the number of ultrasonic pulses to be applied on the specimen, the duration of the pulse and the time delay between two consecutive pulses.

2. FLIR ResearchIR

   ResearchIR is thermal analysis software package for FLIR thermal cameras. The software is used to control the thermal camera. The camera control functions include recording, image analysis and data-sharing. The user can control the recording start time, frame rate, resolution and the end time. Under the image analysis part, the software has features which shows the statistics of a specific region of the image (maximum and minimum temperature, mean temperature), temporal plots, histograms etc. It is through this software, the images recorded during the experiment is imported for further image processing and analysis.

Aluminum extrusions are used to construct the support structure for the ultrasonic transducer and the composite laminate. The aluminum extrusions are connected to each other perpendicularly to form a support structure for the ultrasonic transducer to be fixed to it so that it does not move from its position during operation. The composite laminate is fixed on a scissor jack lift so that it can be moved with respect to the ultrasonic transducer so that direct contact is maintained throughout the experimentation. The CAD model of the support structure is illustrated below:

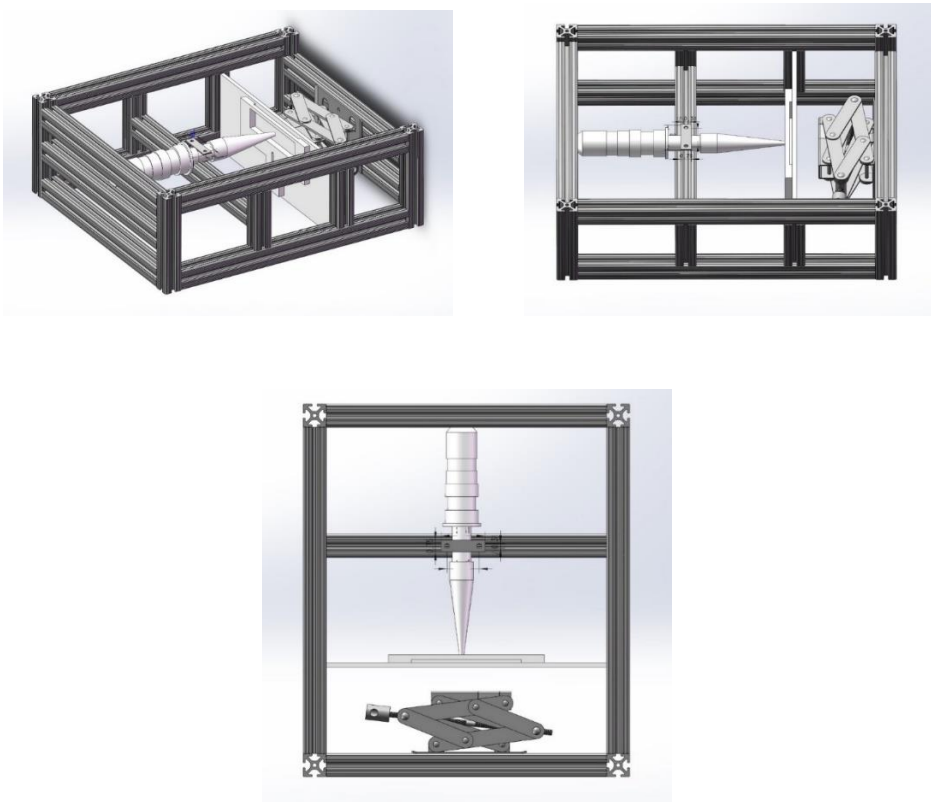

Figure 4: Aluminum Extrusion Support Structure

The following procedure is followed for the setting up the experiment:

1. Connect the ultrasonic transducer to the ultrasonic generator.
2. Connect the multiplexer with the ultrasonic generator as shown below:

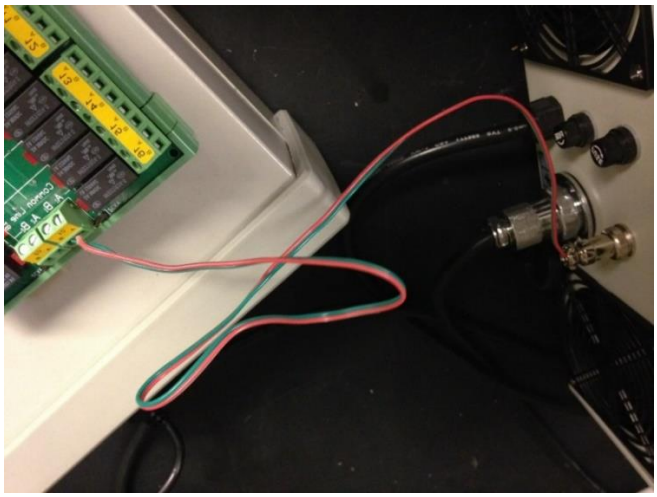

Figure 5: Connection between multiplexer and ultrasonic generator

3. Connect the multiplexer with DC power supply via BNC cables, with computer via USB and press “output” botton on the DC power supply. Set the following values as given below:

   Multiplexer voltage : 24V

   Ultrasonic transducer voltage : 12V

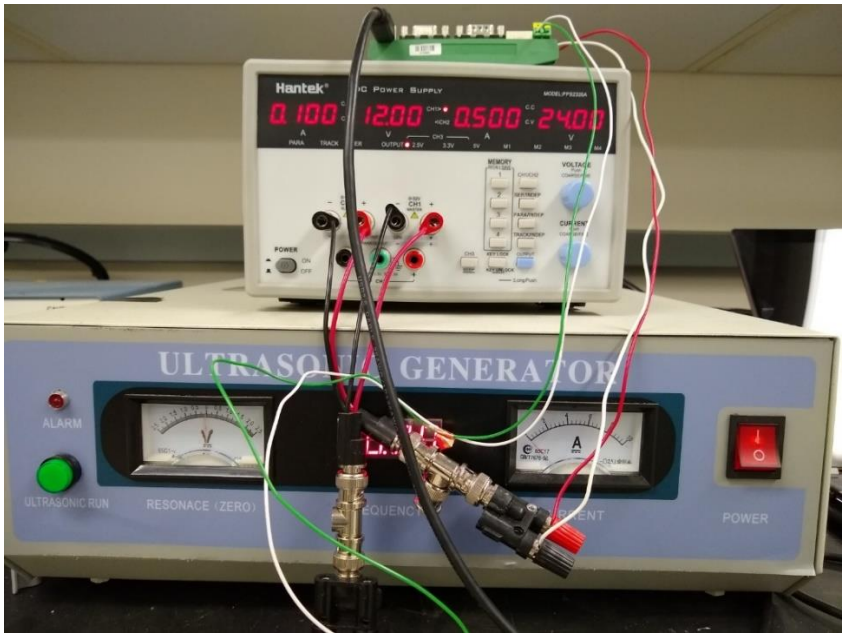

Figure 6: Multiplexer , DC power Supply and Ultrasonic Generator

4. One channel of the muliplexer can be controlled by the labview program.
5. Setup the aluminum extrusions according to the CAD model in Figure 4 and install the composite laminate and ultrasonic transducer accordingly.

The complete experimental setup is illustrated below:

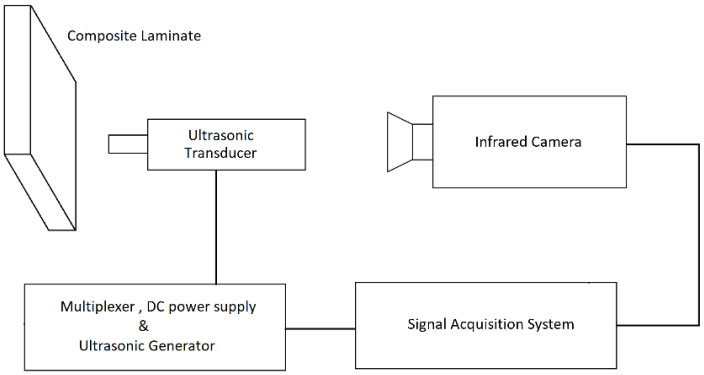

Figure 7: Experimental setup schematic

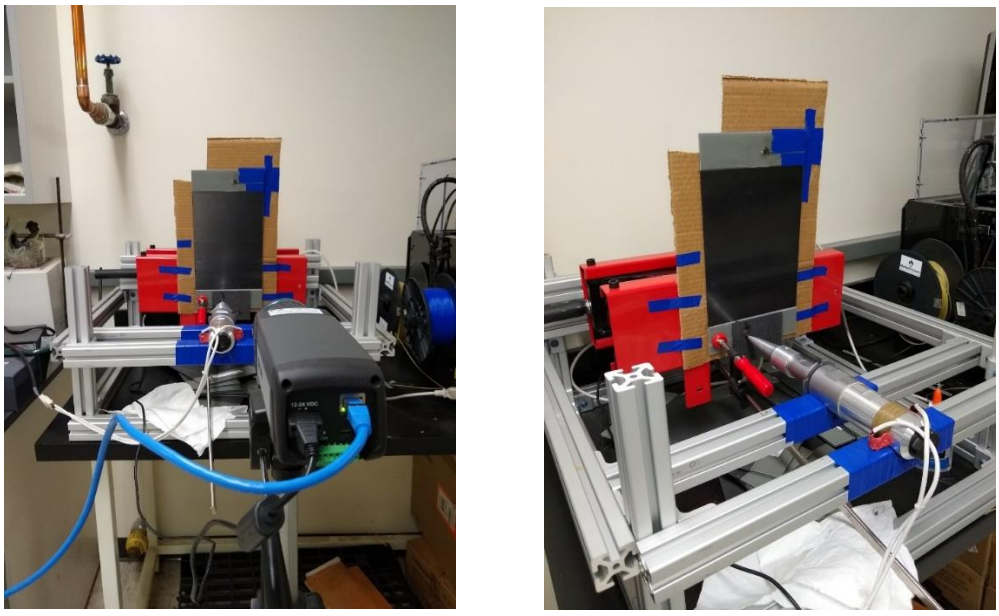

Figure 8: Experimental Setup

2.1

TESTING PROCEDURE

The following procedure is followed for the experimentation and recording of the data through the FLIR ReserachIR software:

1. Use the LABVIEW program designed for this experimentation to set the number of pulses , pulse duration and the time delay between two consecutive pulses.
2. Install the composite laminate on the jack lift and move until the tip of the ultrasonic transducer is in direct contact with it.
3. Using the FLIR ResearchIR software, start recording the video through the infrared camera.
4. Apply the ultrasonic wave through the LABVIEW program immediately after starting the recording. Keep a note of the following:
    a) Keep the camera perpendicular to the surface of the composite laminate.
    b) Make sure the temperature of the surface of the specimen before the testing should be around the minimum value/room temperature.
    c) Glue a piece of wooden plate on the composite laminate at the location where the tip of the transducer touches the laminate. This ensures that the transducer does not damage (burn) the composite laminate in case the experiment parameters are incorrect.

d) Ensure that the ultrasonic transducer is completely insulated from the aluminium support structure during its operation or else it will result in short circuit.

e) Don’t let the ultrasonic transducer burn the specimen.

5. Manually fix the minimum and maximum temperature in the ResearchIR software so that the warm objects in the image are clearly visible.
6. After the experimentation , export the video as multiple images using the software features shown below:
7. Store the images in the computer and use it for the image processing and further analysis.

2.2

RAW EXPERIMENTAL DATA

Using the thermal camera and ResearchIR software package, the change in the surface temperature of the composite laminate is recorded. After the NDE experiment, the video recorded during the experimentation is exported as multiple images which will be used for further image analysis and processing in the later sections of this research.

The software package has various features through which we can analyze the video recorded during the testing. The primary data required is the temperature – time curve of the different defect delaminations in the composite laminate to study the temperature change for the time ultrasonic pulse is applied to the composite laminate.

The software also allows to determine the temperature statistics for the entire period of experimentation of the entire image and for some specific areas of the image. For determining the temperature statistics of a specific region of the image, the Region of Interest (ROI) tool is used. The ROI tool enables the user to draw a region which can be a shape of choice (rectangle, circle etc.) over the area of interest of user defined size. The user can simply view the temporal plot (temperature-time curve), histogram, statistical temperature data for that region at any point of time in the experimentation.

The procedure for obtaining the experimental data is described below:

1) Setup the experimental setting as described in the previous section. Also, set the values of the process parameters as required in the LABVIEW program.

2) Start recording the video using the Research IR software package and then start the experiment. This includes using the LABVIEW program to start the ultrasonic pulse signal.
3) After the experiment ends, the video can be saved in the computer.
4) Open the video file using the ResearchIR software package.
5) The temperature at any point on the image and at any time can be obtained by the position the cursor at the desired position.
6) Using the ROI tool draw the region around the defect area as visible in the image at a suitable time.
7) Using the Statistics Viewer feature, the temperature statistics can be obtained for each of the ROI area in the image.
8) Using the Temporal Plot feature, the temporal plot (temperature-time curve) for each of the ROI area in the image can be obtained and exported as an excel datasheet also for further analysis.

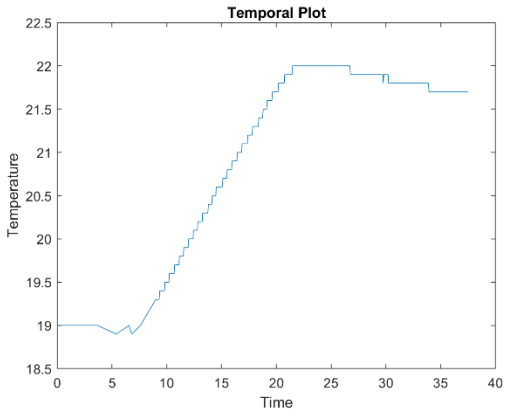

Figure 9: Temporal Plots

2.3

PROBABILITY OF DETECTION (POD)

In deterministic analysis, the defect size/dimension or defect characteristic detected through the SONIC IR testing is always a single value. In probabilistic approach, the defect characteristic is estimated to be a range following an assumed distribution. In practice, the defect characteristics like size, depth etc. are always probabilistic in nature. The ability to detect defects using a non-destructive method is quantified using a statistical parameter called “Probability of Detection (POD)”. Simply put, POD is the probability of detecting a detect of a size/characteristic. POD is used to quantify the reliability of the NDT method.

In this study, two types of composite laminates with defect delaminations of different length and at different depths of the laminate have been used to evaluate the relationship between the POD function and the defect features under given experimental conditions. Through the experiment, the thermal response signal of different defects is determined. Thermal response signal can be defined as the maximum temperature difference between the defect area and the background area. Based on this data, the POD model is defined and Maximum Likelihood Estimation (MLE) is used to estimate the parameters of the POD model. Also, the confidence bounds of the POD curve is determined to obtain important defect characteristics.

For the D type composite laminate, the diameter of the circular defect and side length of the rectangular defects is considered as the defect dimension ‘a’ for the study since all the three defects are present at the same depth.

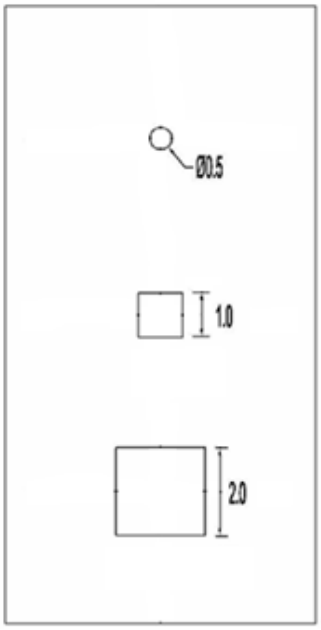

Figure 10: D type composite laminate

Below is the data observed from the SONIC IR experiment.

Defect Dimension (a), mm	Response Signal, (^{o}C)
12.7 mm	1.7
25.4 mm	4.2
50.8 mm	5.1

Table 2: Response Signal Data

The POD function can be obtained from the relationship between 'a' and 'a_r'. As we can observe from the above graphs, the linear relation between the response signal and defect dimension can be expressed as [17]:

$$\ln(a_r) = \beta_o + \beta_1 \ln(a) + \varepsilon \tag{27}$$

a_r = Response Signal (^oC)

a = Defect dimension (mm)

β_o = Intercept of the regression line

β_1 = Slope of the regression line

ε = Error term

The values of β_o, β_1 are calculated using Maximum Likelihood Estimation (MLE). Using linear regression analysis, we can observe that ε follows normal distribution with zero mean value and standard deviation τ.

The POD for defect of length a is given by [17]:

$$\mathrm{POD}(a) = \Phi\left(\frac{\ln(a) - \mu}{\sigma}\right) \tag{28}$$

μ = mean value of the log defect length

σ = standard deviation value of the log defect length

$$\mu = \frac{\ln(a_{th}) - \beta_o}{\beta_1} \tag{29}$$

$$\sigma = \frac{\tau}{\beta_1} \tag{30}$$

The term a_{th} is called the response signal decision threshold value. When the response signal a_r of a defect is greater than a_{th}, it is considered a defect. For this calculation, the value of a_{th} is equal to 1.5 ^{o}C.

Using Maximum Likelihood Estimation, a random variable X is defined, which follows a standard normal distribution [17]:

$$X = \frac{\ln(a_r) - (\beta_o + \beta_1 \ln(a))}{\tau} \tag{31}$$

The probability density function (PDF) of X is given by [17]:

$$\phi(X) = \frac{1}{\sqrt{2\pi}} \exp\left(\frac{-X^2}{2}\right) \tag{32}$$

The likelihood function is [17]:

$$L = \prod_{i=1}^{n} \frac{1}{\tau} \phi(x_i) \tag{33}$$

Log of the likelihood function is given by [17]:

$$\ln(L) = -n\ln(\tau) - \frac{1}{2\tau^2} \sum_{n} [\ln(a_{ri}) - (\beta_o + \beta_1 \ln(a_i))] \tag{34}$$

n is the number of defects in the composite laminate.

The MLE of the POD function are given by the equations given below [17]:

$$\frac{\partial \ln(L)}{\partial \beta_o} = \frac{1}{\tau} \sum_{i=1}^{n} X_i = 0 \tag{35}$$

$$\frac{\partial \ln(L)}{\partial \beta_1} = \frac{1}{\tau} \sum_{i=1}^{n} \ln(a_i)\, X_i = 0 \tag{36}$$

$$\frac{\partial \ln(L)}{\partial \tau} = \frac{1}{\tau} \left(-n + \sum_{i=1}^{n} X_i^2 \right) = 0 \tag{37}$$

Solving the three equations above,

$$\beta_o = -1.365302$$

$$\beta_1 = 0.7925$$

$$\tau = 0.16744$$

$$\mathrm{POD}(a) = \Phi\left(\frac{\ln(a) - \mu}{\sigma}\right)$$

$$\mu = \frac{\ln(a_{th}) - \beta_o}{\beta_1} = \frac{\ln(1.5) - (-1.365302)}{0.7925} = 2.2344$$

$$\sigma = \frac{\tau}{\beta_1} = \frac{0.16744}{0.7925} = 0.21166$$

a = 12.7 mm

$$\mathrm{POD}(a = 12.7) = \Phi\left(\frac{\ln(a) - \mu}{\sigma}\right) = \Phi\left(\frac{\ln(12.7) - 2.2344}{0.21166}\right) = \Phi(1.4518) = 0.92647$$

a = 25.4 mm

$$\mathrm{POD}(a = 25.4) = \Phi\left(\frac{\ln(a) - \mu}{\sigma}\right) = \Phi\left(\frac{\ln(25.4) - 2.2344}{0.21166}\right) = \Phi(4.7299) = 0.9999$$

a = 50.8 mm

$$\mathrm{POD}(a = 50.8) = \Phi\left(\frac{\ln(a) - \mu}{\sigma}\right) = \Phi\left(\frac{\ln(50.8) - 2.2344}{0.21166}\right) = \Phi(8.005) \cong 1$$

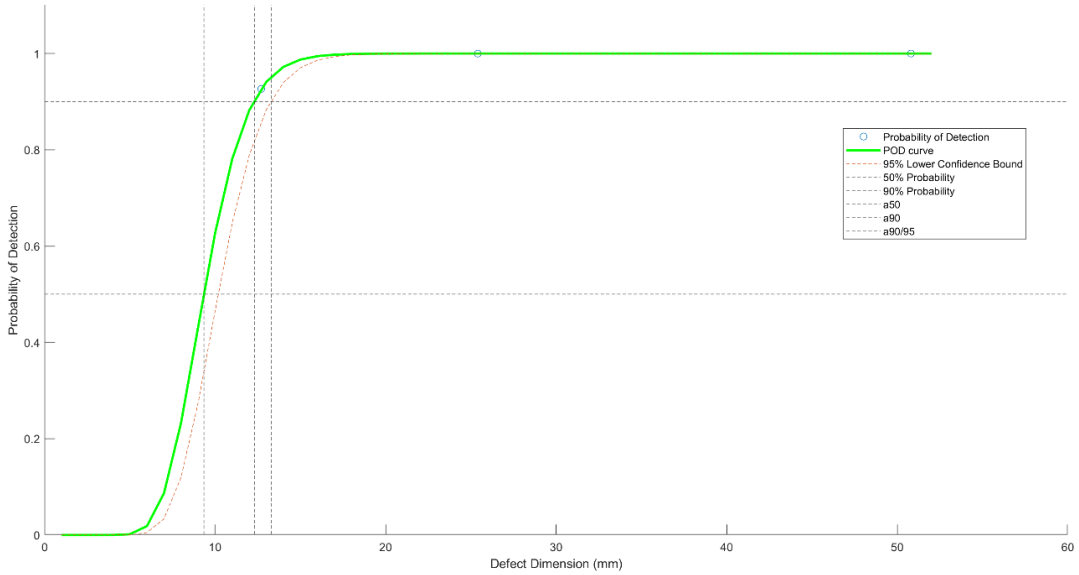

Figure 11: POD Curve for D type Laminate

The lower 95% confidence bound of the POD curve is determined to find the following parameters of the defects:

1. $a_{90/95}$

   $a_{90/95}$ is defined as the defect depth which can be detected with a 90% probability within the confidence bound of 95%.

2. a_{50}

   a_{50} is defined as the defect depth which can be detected with a 90% probability.

3. a_{90}

   a_{90} is defined as the defect depth which can be detected with a 95% probability.

Using the POD curve, we can obtain the value of a_{50}, a_{90}, $a_{90/95}$.

From the POD curve above,

a_{50} = 9.35 mm

a_{90} = 12.3016 mm

$a_{90/95}$ = 13.292 mm

For the E type laminate, the defects are present different depths of the composite laminate.

In this case, the defect depth is considered as the main parameter for the study.

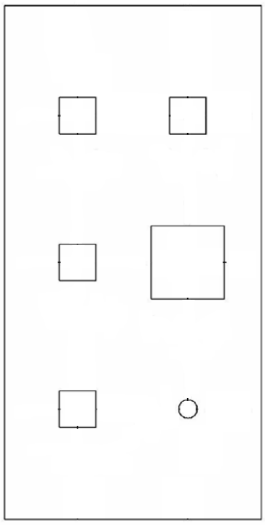

Figure 12: E type composite laminate

Defect Depth (d), µm	Response Signal, (°C)
0.296	7.1
0.296	3.9
0.592	3.1
0.888	4
1.184	2.8
1.48	1.9

Table 3: Response Signal Data

The linear model given below can be used for the POD analysis:

$$\ln(a_r) = \beta_o + \beta_1 \ln(d) + \varepsilon$$

d = Defect Depth (µm)

Similar to the POD analysis for the D type composite laminate, values of the parameters can be obtained by solving the equations given below:

$$\frac{\partial \ln(L)}{\partial \beta_o} = \frac{1}{\tau} \sum_{i=1}^{n} X_i = 0$$

$$\frac{\partial \ln(L)}{\partial \beta_1} = \frac{1}{\tau} \sum_{i=1}^{n} \ln(a_i) X_i = 0$$

$$\frac{\partial \ln(L)}{\partial \tau} = \frac{1}{\tau} \left(-n + \sum_{i=1}^{n} X_i^2 \right) = 0$$

$\beta_o = 1.1587$

$\beta_1 = -0.61354$

$\tau = 0.19316$

For this case $a_{th} = 1.8\ ^oC$

$$\mu = \frac{\ln(a_{th}) - \beta_o}{\beta_1} = \frac{\ln(1.8) - 1.1587}{-0.61354} = 0.9305$$

$$\sigma = \frac{\tau}{\beta_1} = \frac{0.19316}{0.61354} = 0.314822$$

d = 0.296 mm

$$\mathrm{POD}(d = 0.296) = \Phi\left(\frac{\ln(d) - \mu}{\sigma}\right) = \Phi\left(\frac{\ln(0.296) - 0.9305}{-0.314822}\right) = \Phi(6.82) \cong 1$$

d = 0.592 mm

$$\mathrm{POD}(d = 0.592) = \Phi\left(\frac{\ln(d) - \mu}{\sigma}\right) = \Phi\left(\frac{\ln(0.592) - 0.9305}{-0.314822}\right) = \Phi(4.62) = 0.9999$$

d = 0.888 mm

$$\mathrm{POD}(d = 0.888) = \Phi\left(\frac{\ln(d) - \mu}{\sigma}\right) = \Phi\left(\frac{\ln(0.888) - 0.9305}{-0.314822}\right) = \Phi(3.3) = 0.99957$$

d =1.184 mm

$$\mathrm{POD}(d = 1.184) = \Phi\left(\frac{\ln(d) - \mu}{\sigma}\right) = \Phi\left(\frac{\ln(1.184) - 0.9305}{-0.314822}\right) = \Phi(2.419) = 0.992$$

d =1.48 mm

$$\mathrm{POD}(\mathrm{d}=1.48)=\Phi\left(\frac{\ln(\mathrm{d})\ -\ \mu}{\sigma}\right)=\Phi\left(\frac{\ln(1.48)\ -\ 0.9305}{-0.314822}\right)=\Phi(1.710)=0.956$$

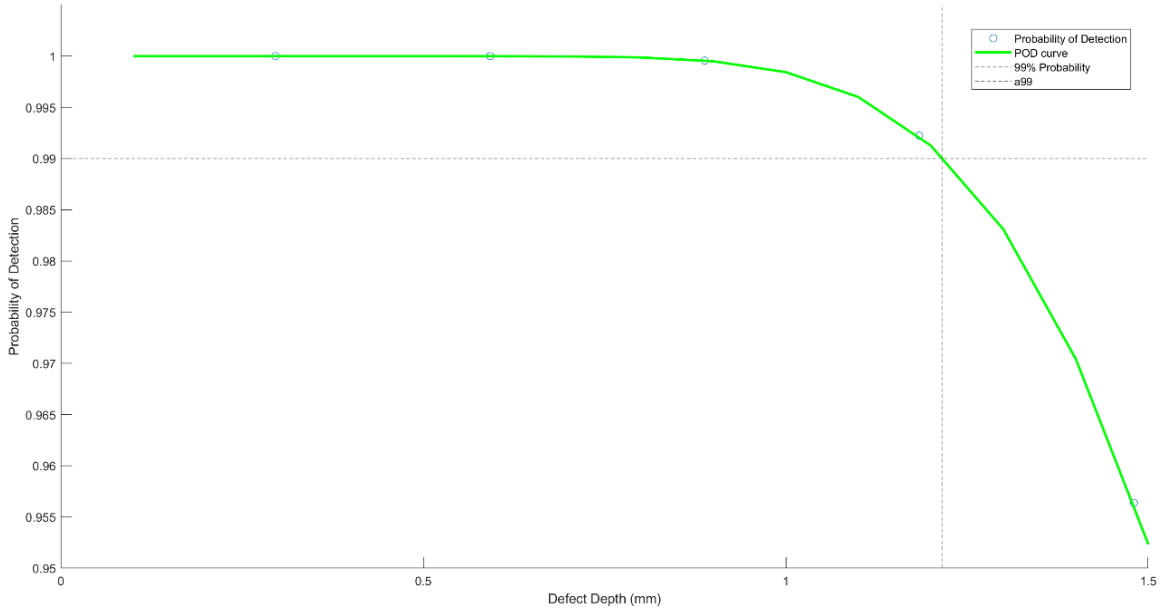

Figure 13: POD Curve for E type laminate

From the POD curve,

d_{99} = 1.2154 mm

d_{99} is defined as the defect depth which can be detected with a probability of 99%.

CHAPTER 3

DEFECT DETECTION ALGORITHMS

Image analysis and processing is used to extract and identifying objects and patterns in the image. Image analysis involves the conversion of features in the image into quantitative data.

The main objective of this non-destructive testing is to identify the defects and delaminations present in the composite laminate. To distinguish the defects from the background of the thermal image obtained from IR camera, we use thermal image analysis. Thermal image analysis includes algorithm which is used to detect the location and characteristics of the defect.

The algorithms for defect detection are categorized into two categories: nondedicated and dedicated algorithms. A nondedicated algorithm is an algorithm which is not specifically designed for defect detection in thermal images, whereas a dedicated algorithm is an algorithm which is specifically designed to work on a thermal image. In the next two sections, some of the existing dedicated and non-dedicated algorithms are discussed and used for thermal image processing.

The exact defect location and the dimensions of the composite laminates are illustrated in the figure below:

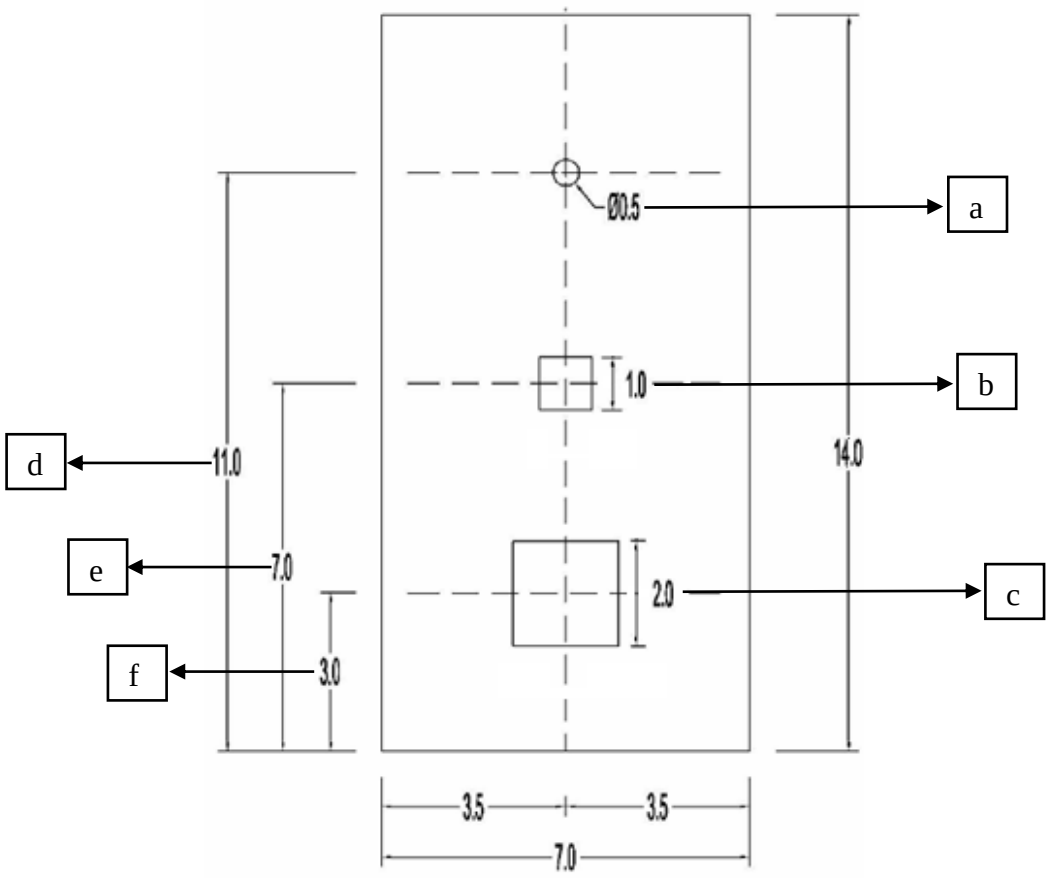

Figure 14: D type composite laminate

a: Diameter of the circle

b: Side Length of the square located at 7” from the bottom of the laminate

c: Side Length of the square located at 3” from the bottom of the laminate

d: Distance between the center of the circle and the bottom of the laminate

e: Distance between the center of the 1” square and the bottom of the laminate

f: Distance between the center of the 2” square and the bottom of the laminate

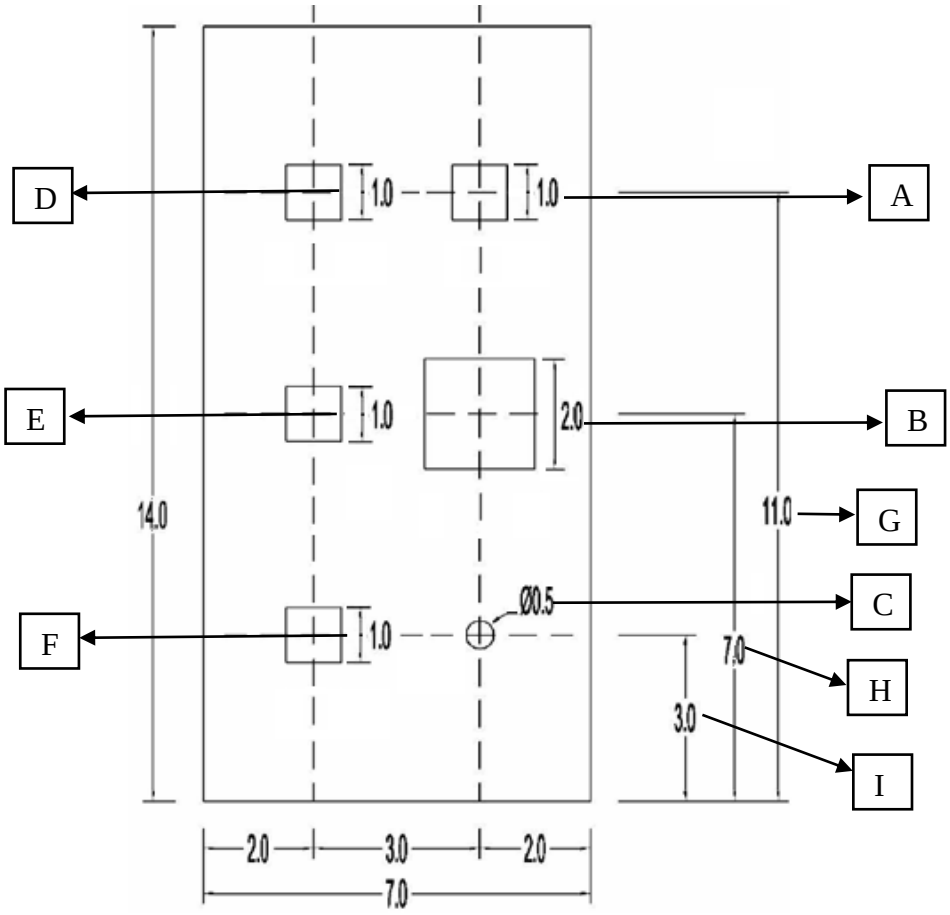

Figure 15: E type composite laminate

A: Side Length of the square located at 11” from the bottom of the laminate

B: Side Length of the square located at 7” from the bottom of the laminate

C: Diameter of the circle

D: Side Length of the square located at 11” from the bottom of the laminate

E: Side Length of the square located at 7” from the bottom of the laminate

F: Side Length of the square located at 3” from the bottom of the laminate

G: Distance between the center of the 1” square and the bottom of the laminate

H: Distance between the center of the 2” square and the bottom of the laminate

I: Distance between the center of the circle” square and the bottom of the laminate

The infrared images of the composite plate during the SONIC IR testing captured by the IR camera are shown below:

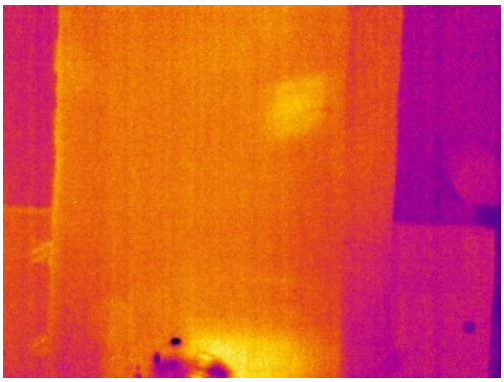

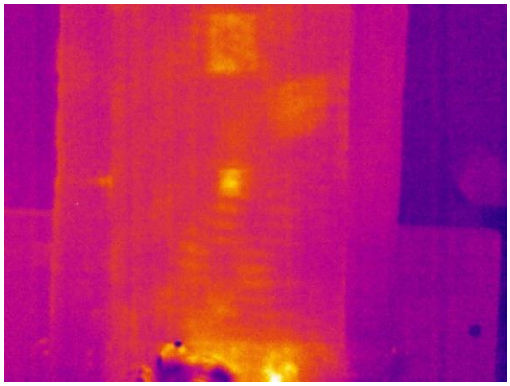

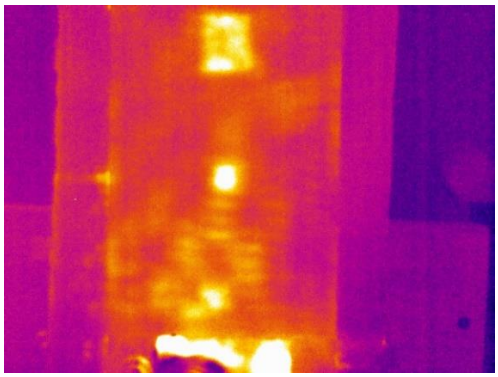

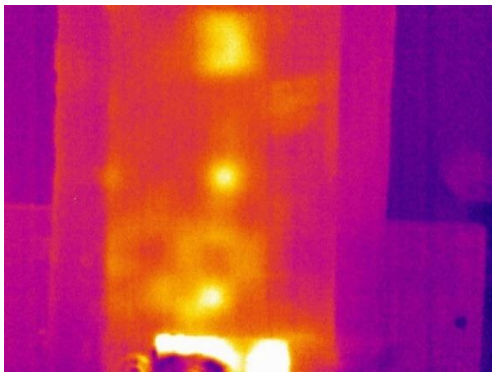

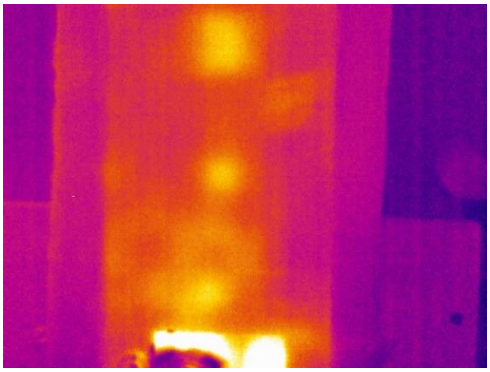

Figure 16: Thermal images obtained throughout the experimentation

Note: The bright area in the lower part of the image represents the actuation area where the sonic pulse is applied therefore the temperature increase is maximum in that region. It can be observed that the thermal images get blurrier as the heating time increases. The optimal time at which the defects can be obtained accurately is between 10 s to 18 s.

The thermal image analysis will be conducted on the images below:

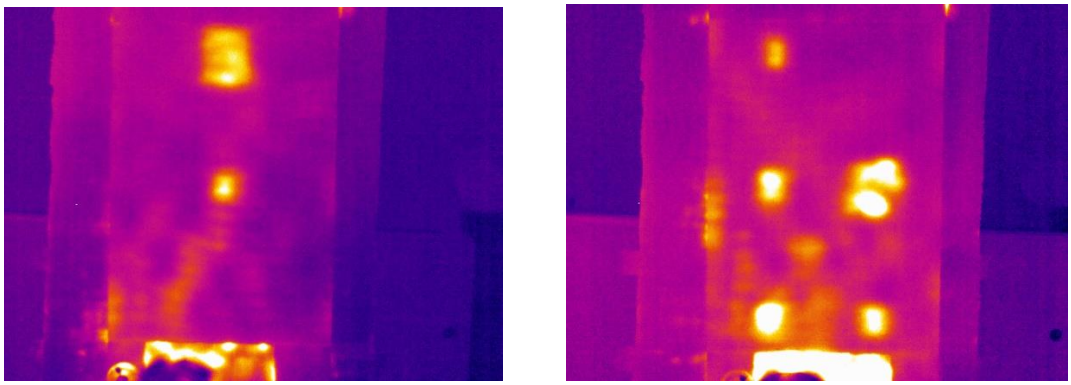

Figure 17: Thermal IR Images

3.1
NON-DEDICATED ALGORITHMS

1. Otsu Algorithm

According to Otsu's method, the threshold is selected by maximizing the between-class variances.

Let F = {f_1, f_2, f_3,….,f_{MxN}} represent the gray level image of size M x N where fi ϵ [1,2,….,L-1] is the gray value of the i^{th} pixel of the image [14] . If the number of pixels with gray level g is f(g), then the probability of occurrence of gray level g is given as [14]:

$$p(g) = \frac{f(g)}{M \text{ x } N} \text{ , } g = 0,1,2, \ldots\ldots, L-1 \tag{38}$$

The average gray level of the entire image is [14]:

$$\mu_T = \sum_{g=0}^{L-1} g.\, p(g) \tag{39}$$

Dividing the pixels of the image into two classes (object and background or background and object) [14]:

$$C_0 = \{0, 1, 2, 3,\ldots\ldots, T\}$$

$$C_1 = \{T+1, T+2,\ldots\ldots,L-1\} \tag{40}$$

T is the threshold value.

The probabilities of these two classes are [14]:

$$p_0(T) = \sum_{g=0}^{T} p(g) \tag{41}$$

$$p_1(T) = \sum_{g=T+1}^{L-1} p(g) \tag{42}$$

The mean value of each class is computed as [14]:

$$\mu_0(T) = \sum_{g=0}^{T} \frac{g.\,p(g)}{p_0(T)} \tag{43}$$

$$\mu_1(T) = \sum_{g=T+1}^{L-1} \frac{g.\,p(g)}{p_1(T)} \tag{44}$$

Also,

$$p_0(T)\mu_0(T) + p_1(T)\mu_1(T) = 1 \tag{45}$$

The between class variance of C_0 and C_1 is [14]:

$$\sigma_B^2(T) = p_0(T)[\mu_0(t) - \mu_T]^2 + p_1(T)[\mu_1(t) - \mu_T]^2 = p_0(T)\mu_0^2(T) + p_1(T)\mu_1^2(T) \tag{46}$$

Therefore, the optimal threshold is calculated as [14]:

$$T^* = \arg\max_{0<t<L-1}\sigma_B^2(T) = \arg\max_{0<t<L-1}p_0(T)\mu_0^2(T) + p_1(T)\mu_1^2(T) \quad (47)$$

For D type composite laminate,

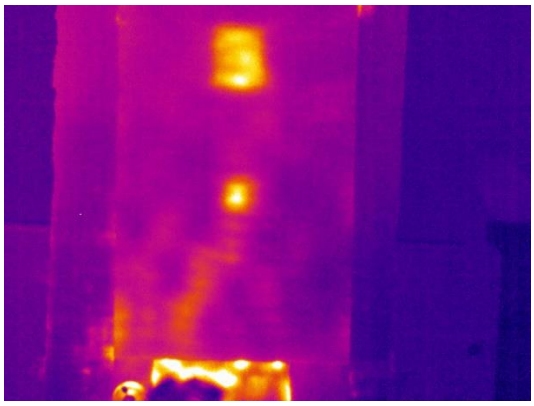

Figure 18: Original thermal image

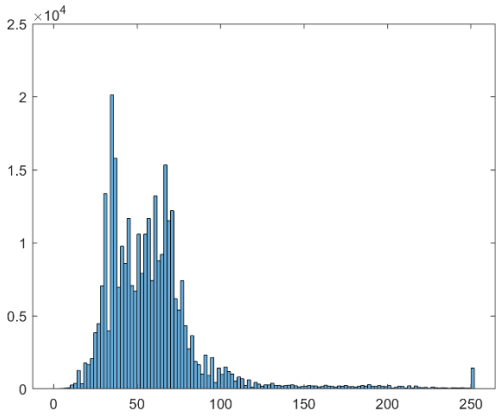

Figure 19: Histogram of the thermal image

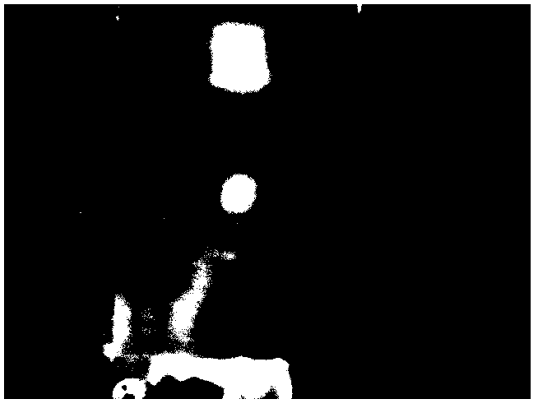

Figure 20: Processed Thermal Image

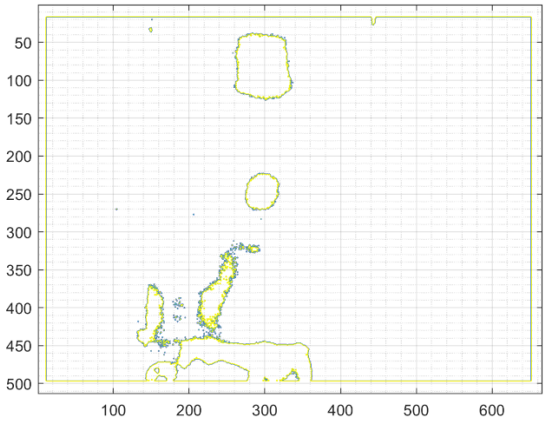

Figure 21: Contour image

Dimension (mm)	Ground Truth (mm)	Image Analysis Value (mm)	Error %
a	12.7	-	
b	25.4	27.5661	8.53
c	50.8	49.0064	3.53
d – 6.35	273.5	-	-
e – 12.7	165.1	156.2286	5.37
f – 25.4	50.8	52.09	2.54

Table 4: Comparison of analysis values and ground truth

Note: The exact location of the centroid of the defect areas cannot be determined accurately. Therefore, the distance from the lower edge of the defects are considered for comparison.

As observed, the circular defect of diameter 0.5'' cannot be detected using this method.

For E type composite laminate,

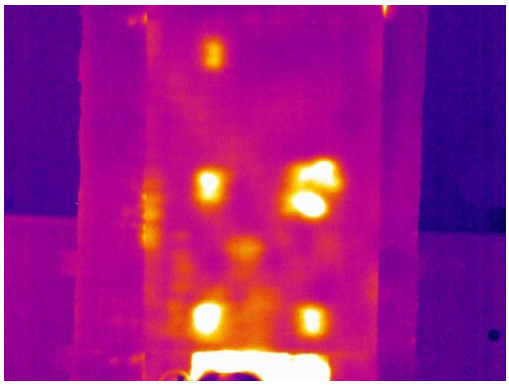

Figure 22: Original Thermal Image

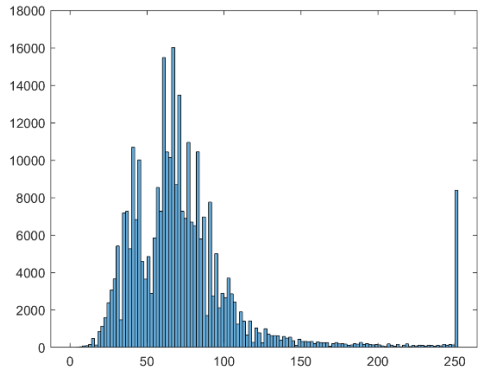

Figure 23: Histogram of the thermal image

Figure 24: Processed Thermal Image

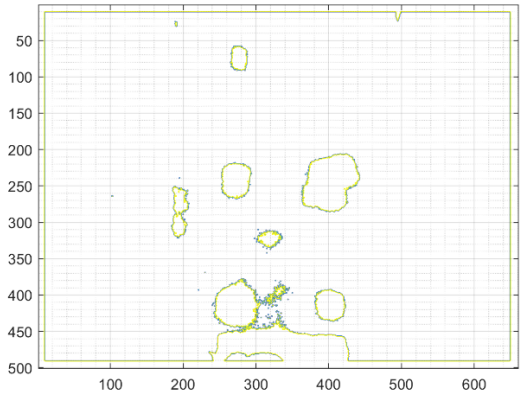

Figure 25: Contour image

Dimension (mm)	Ground Truth (mm)	Image Analysis Value (mm)	Error %
A	25.4	25.116	1.11
B	50.8	47.84	5.83
C	12.7	-	-
D	25.4	35.98	41.65
E	25.4	26.91	5.94
F	25.4	20.93	17.6
G – 12.7	266.7	215.28	19.28
H – 25.4	152.4	107.64	29.37
I – 6.35	69.85	-	-

Table 5: Comparison of analysis values and ground truth

As observed, the circular defect of diameter 0.5’’ cannot be detected using this method.

2. Tsai Algorithm

This is an algorithm based on the moment-preserving principle [9]. The gray level moments of the input image are calculated. The thresholds are selected such that the moments of the thresholded image are preserved.

For an image f with n pixels, the gray level for the pixel located at (x,y) is denoted by f(x,y). The image is thresholded into two-pixel classes: the below-threshold pixels and above-threshold pixels. The i^{th} moment of image f is given by [9]:

$$m_i = \frac{1}{n}\sum_x \sum_y f_i(x,y) \quad , i = 1,2,3,4 \ldots . \tag{48}$$

Moment can be calculated from the gray level histogram of the image as [9]:

$$m_i = \frac{1}{n}\sum_j n_j \left(z_j\right)^i$$

$$= \sum_j p_j \left(z_j\right)^i \tag{49}$$

n_j is the number of pixels in the image f with gray value z_j. The value of m_0 is assumed to be 1. Image f has pixels which has only two gray values: z_0 and z_1 and $z_0 < z_1$. Threshold value is selected such that if all the below-threshold gray values are replaced by z_0 and above-threshold gray values are replaced by z_1, then the first three moments of image f are preserved and a bilevel image g is obtained [9].

If p_0 and p_1 denote the below-threshold pixels and above threshold pixels in the image f, the first three moments of g are [9]:

$$m_i' = \sum_{j=0}^{1} p_j (z_j)^i , i = 1,2,3 \tag{50}$$

Preserving the first three moments in g implies [9]:

$$m_i = m_i', \quad i = 1,2,3 \tag{51}$$

$$p_0 + p_1 = 1 \tag{52}$$

The equalities which is obtained through the above equalities are [9]:

$$p_0 z_0^0 + p_1 z_1^0 = m_0$$

$$p_0 z_0^1 + p_1 z_1^1 = m_1$$

$$p_0 z_0^2 + p_1 z_1^2 = m_2$$

$$p_0 z_0^3 + p_1 z_1^3 = m_3 \tag{53}$$

Solving the above 4 equations, the values of p_0, p_1, z_0 and z_1 is determined.

The threshold value is defined as the p0-tile of the histogram of the image f [9]. The value of threshold T can be calculated as [9]:

$$p_0 = \frac{1}{n}\sum_{z_j \le T} n_j \tag{54}$$

For D type composite laminate,

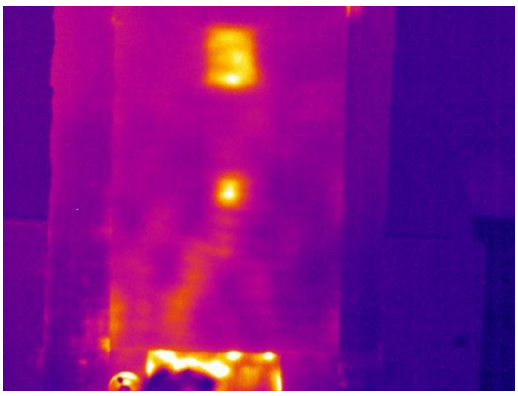

Figure 26: Original Thermal Image

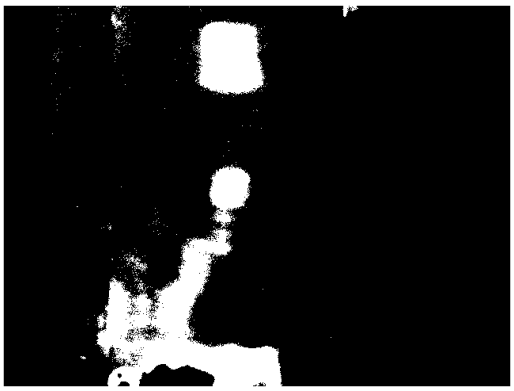

Figure 27: Processed Thermal Image

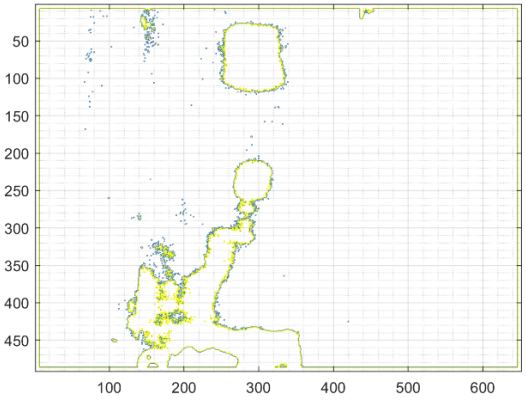

Figure 28: Contour Image

Dimension	Ground Truth (mm)	Image Analysis Value (mm)	Error %
a	12.7	-	-
b	25.4	31.395	23.6
c	50.8	56.511	11.2
d – 6.35	273.5	-	-
e – 12.7	165.1	165.112	0.0073
f – 25.4	50.8	52.09	2.54

Table 6: Comparison of analysis values and ground truth

For E type composite laminate,

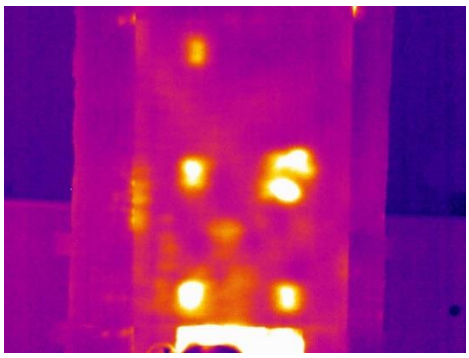

Figure 29: Original Thermal Image

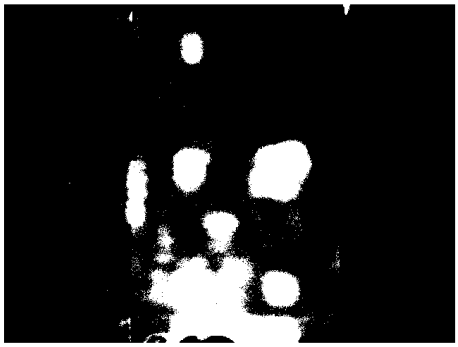

Figure 30: Processed Thermal Image

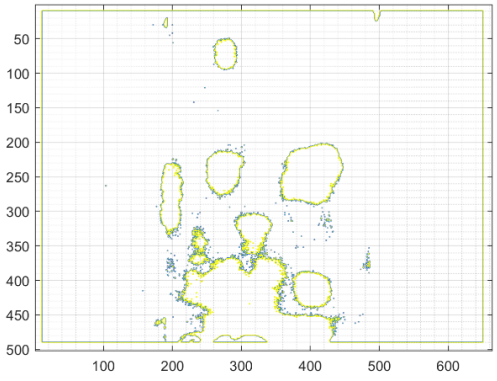

Figure 31: Contour Image

Dimension	Ground Truth (mm)	Image Analysis Value (mm)	Error %
A	25.4	29.9	17.71
B	50.8	50.83	0.059
C	12.7	-	-
D	25.4	-	-
E	25.4	35.88	41.25
F	25.4	25.116	1.11
G – 12.7	266.7	215.28	19.28
H – 25.4	152.4	101.66	33.29
I – 6.35	69.85	-	-

Table 7: Comparison of analysis values and ground truth

3. Niblack Thresholding Algorithm

Niblack Thresholding Algorithm (NBM) is the one of the oldest local thresholding algorithms. Most of the global thresholding algorithms are not able to preserve the minute details of the image in the segmentation process. NBM was proposed to preserve the minute details at a local level introducing the concept of local window rather than global thresholding. The threshold value T can be defined as [10]:

$$T = \mu(x,y) + k*\sigma(x,y) \tag{55}$$

$\mu(x,y)$ is the local mean value of the gray level and $\sigma(x,y)$ is the local standard deviation value of the gray value for a particular local window of the image. k is an image dependent

manually selected parameter. For dark foreground the value of k is considered -0.2 and for 0.2 for dark background. Selecting the value of k manually is one of the drawbacks of this method.

For D type composite laminate,

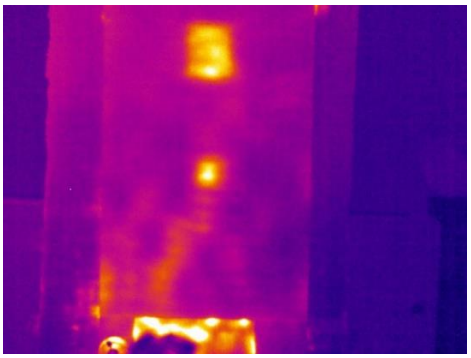

Figure 32: Original Thermal Image

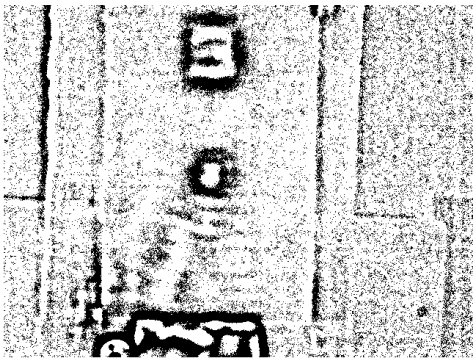

Figure 33: Processed Thermal Image

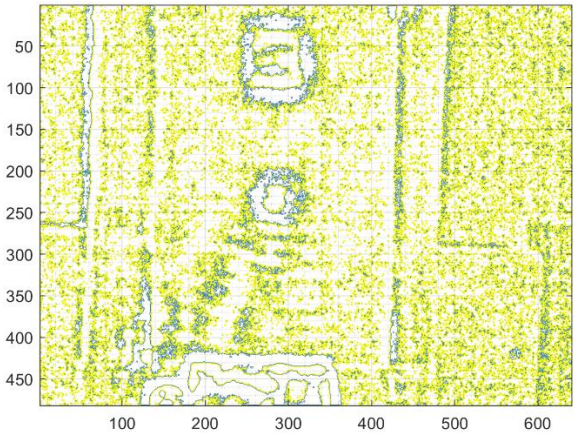

Figure 34: Contour Image

Dimension (mm)	Ground Truth (mm)	Image Analysis Value (mm)	Error %
a	12.7	-	-
b	25.4	18.837	25.84
c	50.8	43.953	13.48
d – 6.35	273.5	-	-
e – 12.7	165.1	75.348	54.36
f – 25.4	50.4	52.09	2.54

Table 8: Comparison of analysis values and ground truth

It can be observed that the contour image has a lot of noise which reduces the accuracy of the method.

For E type composite laminate,

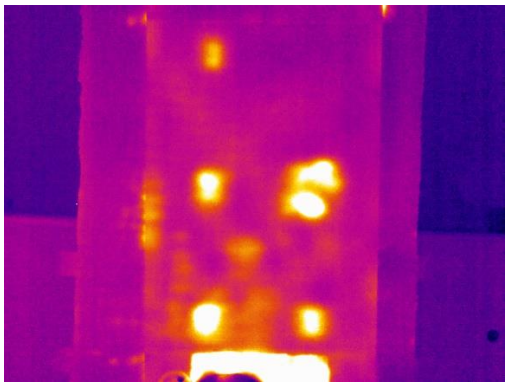

Figure 35: Original Thermal Image

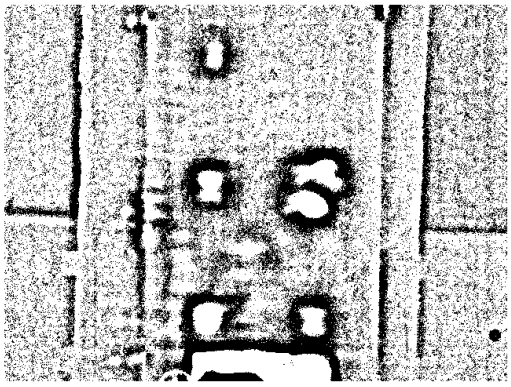

Figure 36: Processed Thermal Image

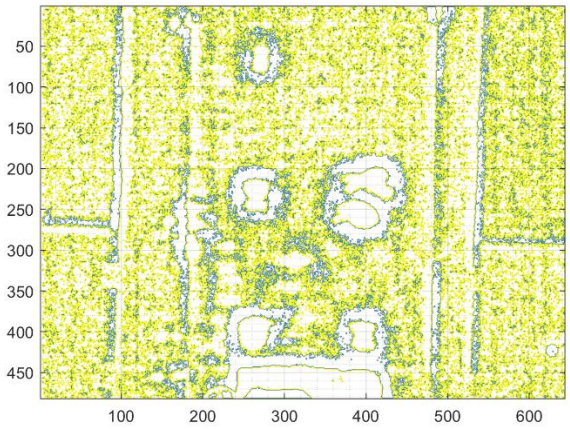

Figure 37: Contour Image

Dimension	Ground Truth (mm)	Image Analysis Value (mm)	Error %
A	25.4	25.116	1.11
B	50.8	47.09	7.3
C	12.7	-	-
D	25.4	31.395	23.6
E	25.4	25.116	1.11
F	25.4	18.837	25.84
G – 12.7	266.7	226.044	15.24
H – 25.4	152.4	75.348	50.56
I – 6.35	69.85	-	-

Table 9: Comparison of analysis values and ground truth

It can be observed that the contour image has a lot of noise which reduces the accuracy of the method.

3.2

DEDICATED ALGORITHMS

1. Hamadani Algorithm

Hamadani [4] proposed an algorithm based on the statistical properties of the thermal image. The mean value μ and standard deviation σ of the gray level of the image is used to obtain the threshold value. The threshold value T for an image f of size M x N is given by [4]:

$$T = k_1 * \mu + k_2 * \sigma \tag{56}$$

$$\mu = \frac{1}{M * N} \sum_{i=1}^{M} \sum_{j=1}^{N} f(i,j) \tag{57}$$

$$\sigma = \sqrt{\frac{1}{M * N} \sum_{i=1}^{M} \sum_{j=1}^{N} (f(i,j) - \mu)^2} \tag{58}$$

The values of k_1 and k_2 are selected manually. Generally, for low resolution images k_1=1 and k_2 = 1 and for higher resolution images k_1 = 1 or 1.5 and k_2 = 2 yields good results [4]. This algorithm is not automatic as the values of k_1 and k_2 are selected manually.

For D type composite laminate,

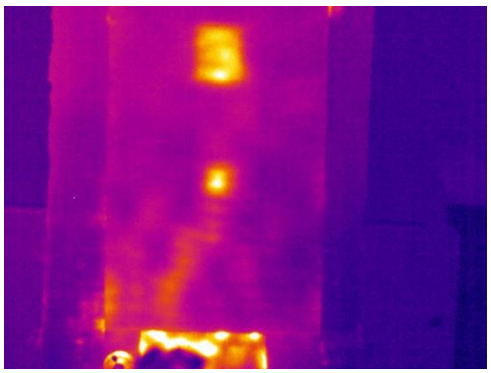

Figure 38: Original Thermal Image

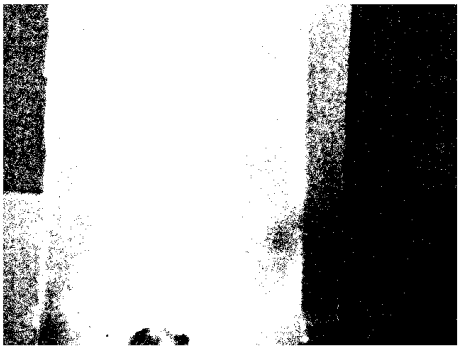

Figure 39: Image for $k_1 = k_2 = 0.5$

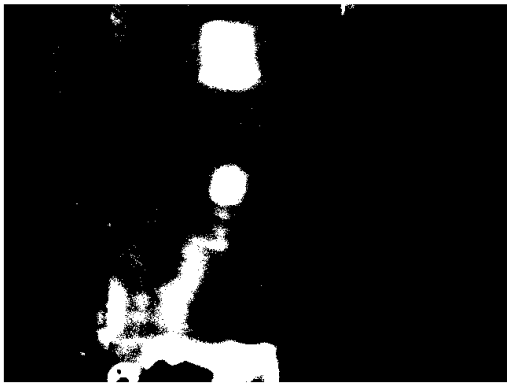

Figure 40: Image for $k_1 = k_2 = 1$

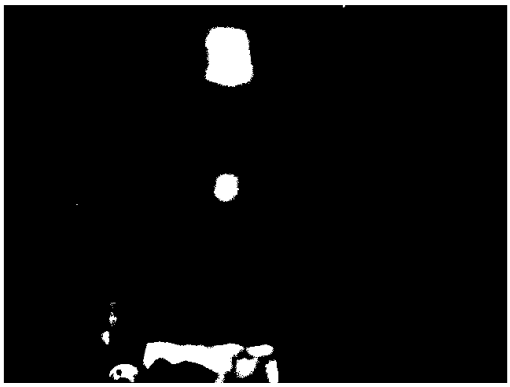

Figure 41: Image for $k_1 = k_2 = 1.5$

Figure 42: Image for $k_1 = k_2 = 2$

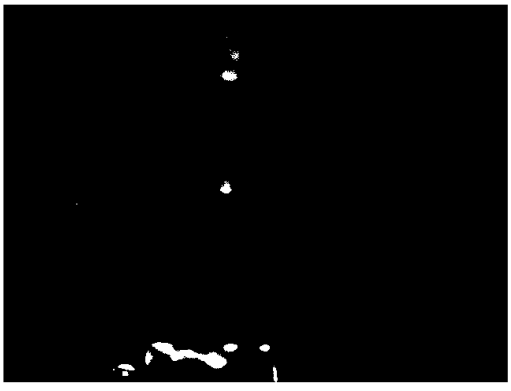

Figure 43: Image for $k_1 = k_2 = 2.5$

It can be observed that the most accurate result is obtained for $k_1 = k_2 = 1.5$.

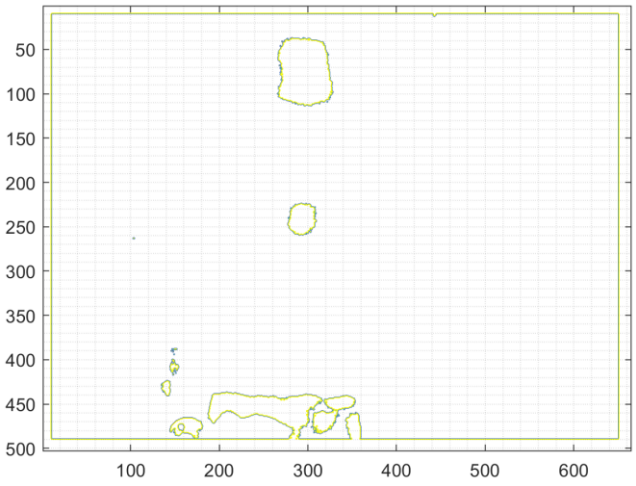

Figure 44: Contour Image for $k_1 = k_2 = 1.5$

Dimension (mm)	Ground Truth (mm)	Image Analysis Value (mm)	Error %
a	12.7	-	-
b	25.4	23.8602	6.063
c	50.8	47.0925	7.29
d – 6.35	273.5	-	-
e – 12.7	165.1	165.112	0.0073
f – 25.4	50.4	52.09	2.54

Table 10: Comparison of analysis values and ground truth

For E type composite laminate,

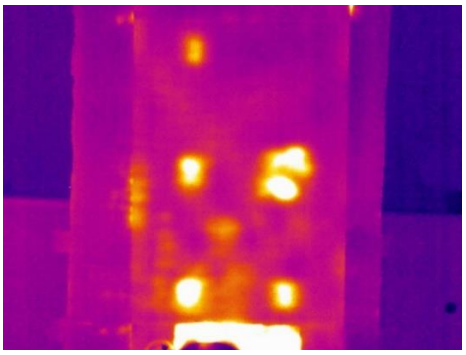

Figure 45: Original Thermal Image

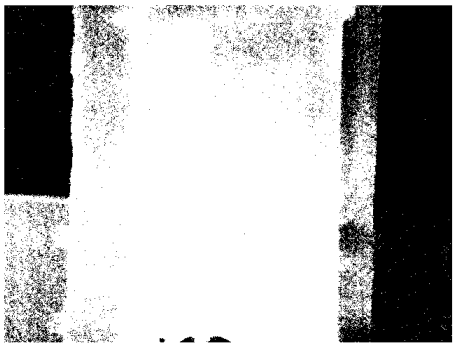

Figure 46: Image for $k_1 = k_2 = 0.5$

Figure 47: Image for $k_1 = k_2 = 1$

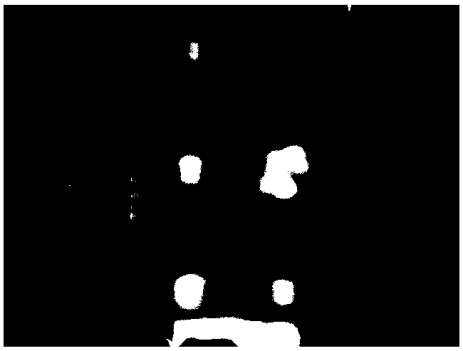

Figure 48: Image for $k_1 = k_2 = 1.5$

Figure 49: Image for $k_1 = k_2 = 2$

Figure 50: Image for $k_1 = k_2 = 2.5$

It can be observed that the most accurate result is obtained for $k_1 = k_2 = 1.5$.

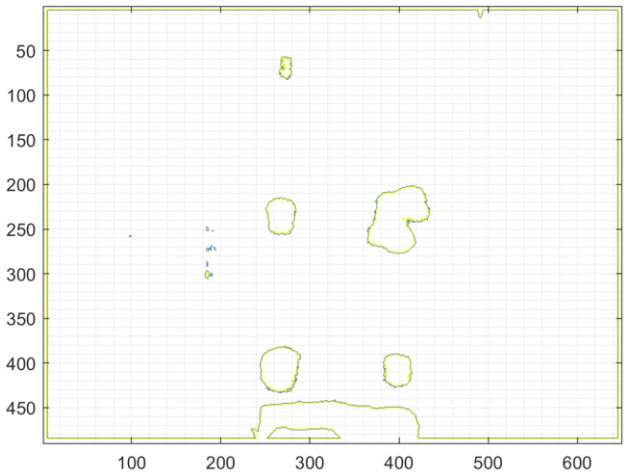

Figure 51: Contour Image for $k_1 = k_2 = 1.5$

Dimension (mm)	Ground Truth (mm)	Image Analysis Value (mm)	Error %
A	25.4	23.92	5.83
B	50.8	47.84	5.83
C	12.7	-	-
D	25.4	28.704	13
E	25.4	23.92	5.83
F	25.4	11.96	52.91
G – 12.7	266.7	215.28	19.28
H – 25.4	152.4	101.66	33.29
I – 6.35	69.85	-	-

Table 11: Comparison of analysis values and ground truth

2. Sapina Method

This method of image analysis comes under the category of dedicated algorithms which is exclusively used for object detection in thermal images. This method uses textural features based on the co-occurrence matrix for distinguishing the warm objects and the background in infrared images. The co-occurrence matrix is a second order statistical method which characterizes the spatial interrelationships of the gray levels in an image [11]. This matrix is used in texture modelling and classification in many applications [11].

The values of the co-occurrence matrix elements present relative frequencies with which two neighboring pixels separated by a distance d appear on the image, where one of the pixels has gray level i and the other has j. This matrix is symmetric and is a function of the angular relationship between two neighboring pixels.

According to the research in [11], the non-normalized frequencies P_{ij} of the co-occurrence matrices for a defined area M x N of the whole image, distance d and angles quantized at 45^o intervals can be defined as [11]:

$$P(I, j, d, 0^o) = \#\{((k,l),(m,n)) \in (MxN)x(MxN) : k-m=0 , |l-n| =d , I(k,l)=I, I(m,n) = j\} \quad (59)$$

$$P(I, j, d, 45^o) = \#\{((k,l),(m,n)) \in (MxN)xMxN) : (k-m=d, l-n=-d) \text{ or } (k-m=-d, 1-n=d), I(k,l)=I, I(m,n) = j\} \quad (60)$$

$$P(I, j, d, 90^o) = \#\{((k,l),(m,n)) \in (MxN)x(MxN) : |k-m| = d, l-n=0 , I(k,l)=I, I(m,n) = j\} \quad (61)$$

P (i, j, d, 135^{o}) = # { ((k,l),(m,n)) ϵ (MxN)x(MxN) : (k-m=d, l-n=d) or (k-m= -d, I-n= -d), I(k,l) = i, I(m,n) =j }

(62)

# denotes the no. of elements in the set.

Using co-occurrence matrix for defining the following textural features given below [11]:

1. Maximum Probability

$$\max_{ij}(P_{ij})$$

(63)

2. Uniformity of Energy

$$\sum_{i} \sum_{j} P_{ij}^{2}$$

(64)

3. Inverse difference moment of order k

$$\sum_{i} \sum_{j} \frac{P_{ij}^{\lambda}}{|i-j|^{k}}$$

(65)

4. Contrast

$$\sum_{i,j} |i-j|^{k} \left(P_{ij}\right)^{\lambda}$$

(66)

5. Variance

$$\left(\sum_{i}(i-\mu_i)^2\sum_{j}P_{ij}\right)\left(\sum_{j}(j-\mu_j)^2\sum_{i}P_{ij}\right) \tag{67}$$

6. Correlation

$$\sum_{i}\sum_{j}\frac{(i-\mu_x)(j-\mu_y)P_{ij}}{\sigma_x\sigma_y} \tag{68}$$

μ_x and μ_y are mean values

$$\mu_x=\sum_{i}i\sum_{j}P_{ij} \tag{69}$$

$$\mu_y=\sum_{j}j\sum_{i}P_{ij} \tag{70}$$

σ_x and σ_y are standard deviation values

$$\sigma_x=\sum_{i}(i-\mu_x)^2\sum_{j}P_{ij} \tag{71}$$

$$\sigma_x=\sum_{j}(j-\mu_y)^2\sum_{i}P_{ij} \tag{72}$$

The infrared images of the two types of composite laminates obtained from the SONIC IR experiment has 256 gray levels. To reduce the time of computation, the gray level is reduced to 64. In both the cases, angle = 45º and the horizontal and vertical displacement are dx = 1 and dy = 1. Below are the images for both the composite laminates:

For D type composite laminate,

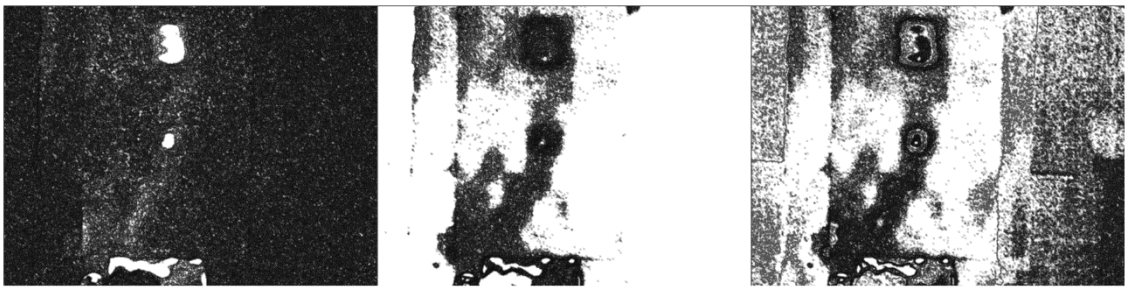

Figure 52: Maximum Probability

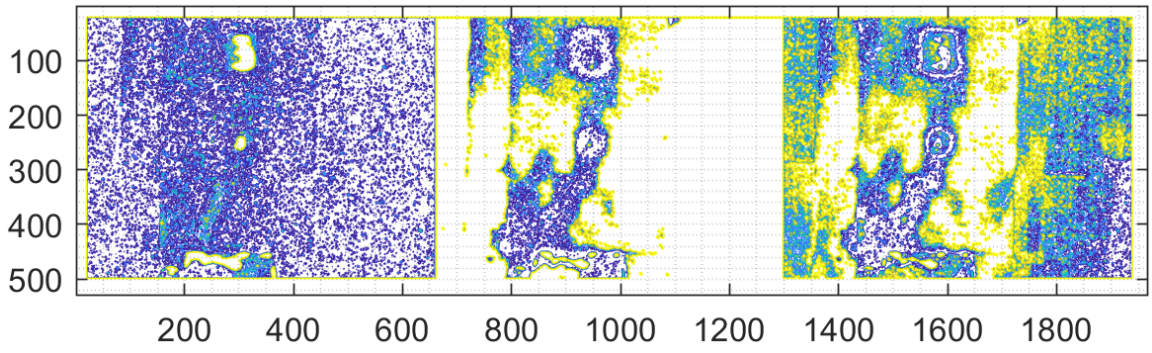

Figure 53: Contour Image for Maximum Probability

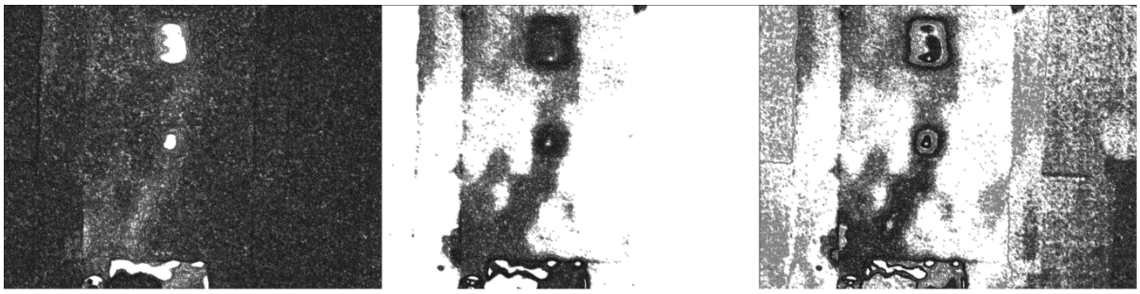

Figure 54: Uniformity of Energy

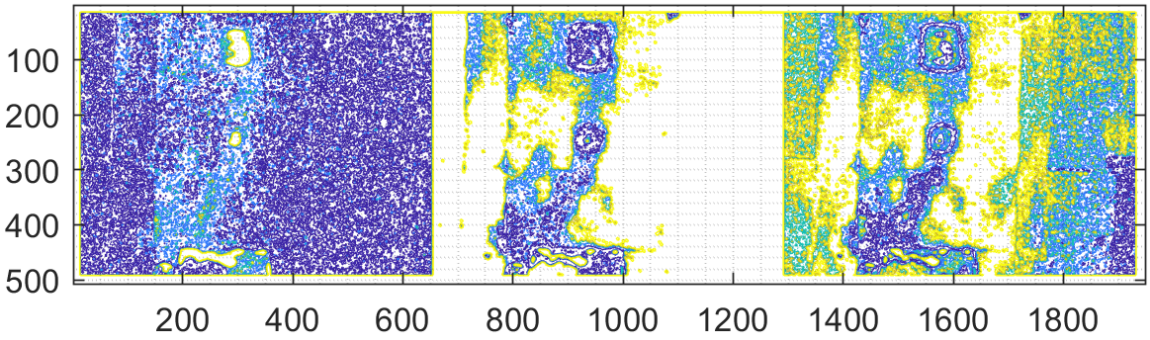

Figure 55: Contour Image for Uniformity of Energy

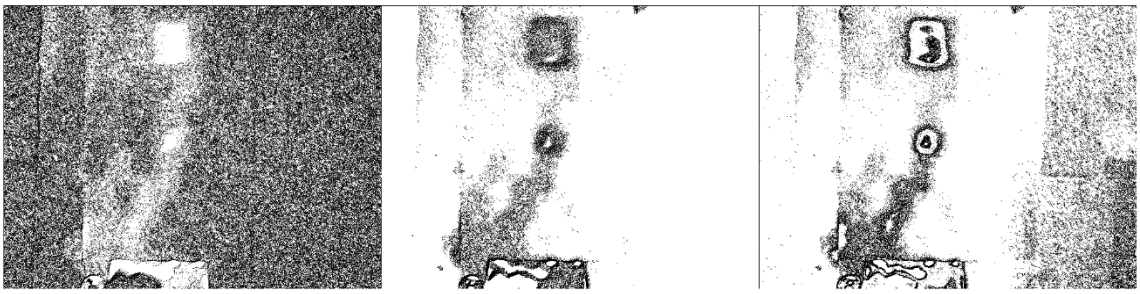

Figure 56: Inverse difference moment of order k

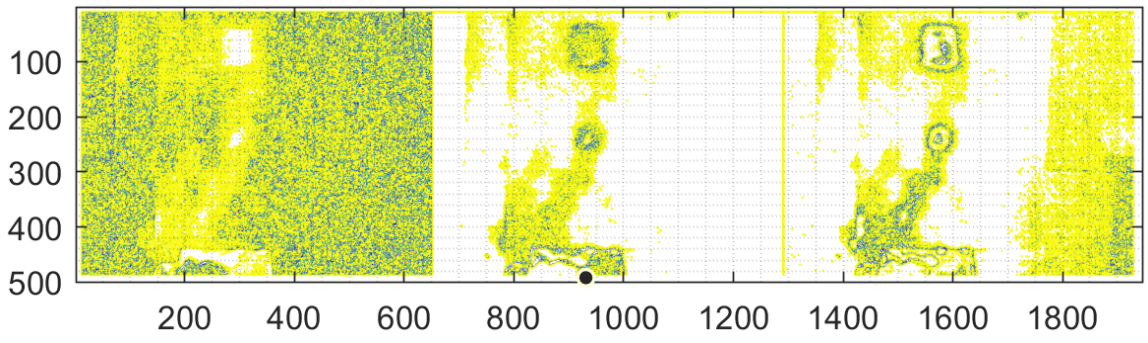

Figure 57: Contour Image for Inverse difference moment of order k

Figure 58: Contrast

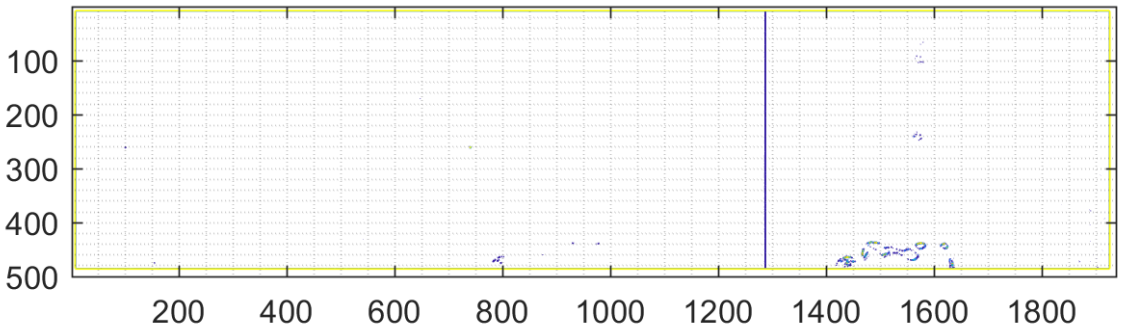

Figure 59: Contour Image for Contrast

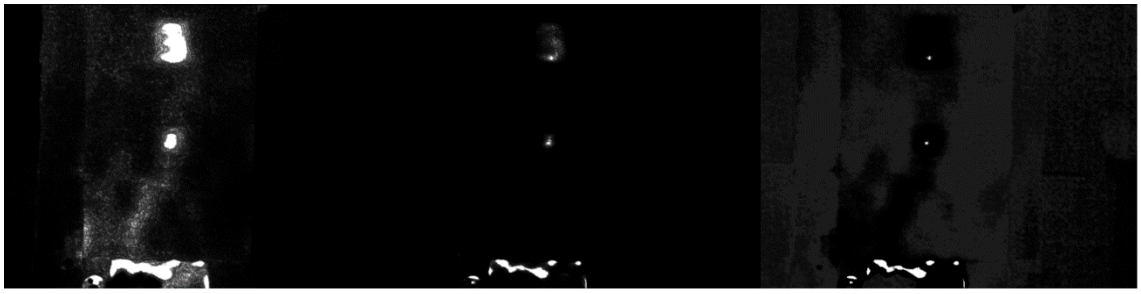

Figure 60: Variance

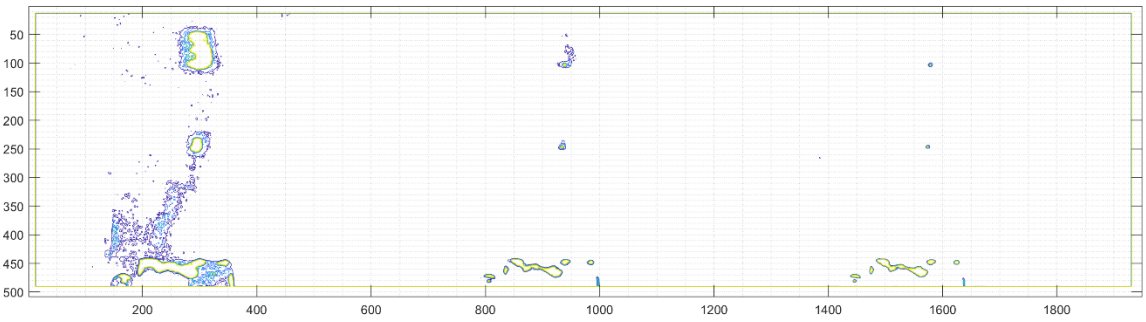

Figure 61: Contour Image for Variance

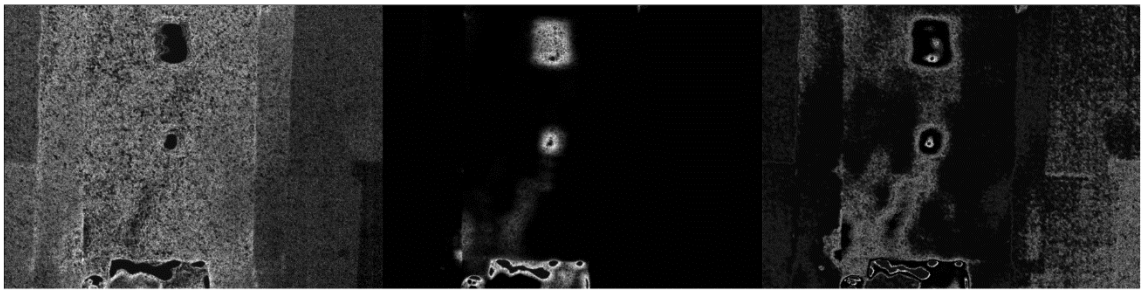

Figure 62: Correlation

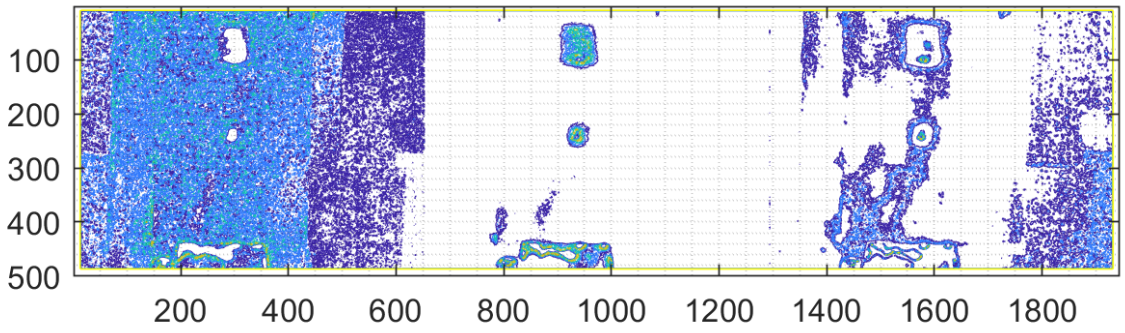

Figure 63: Contour Image for Correlation

As observed from the above images, the correlation textural feature contributes the highest in differentiating the defects in the image.

Dimension	Ground Truth (mm)	Image Analysis Value (mm)	Error %
a	12.7	-	-
b	25.4	25.116	1.118
c	50.8	50.232	1.118
d – 6.35	273.5	-	-
e – 12.7	165.1	113.022	31.543
f – 25.4	50.4	52.09	2.54

Table 12: Comparison of analysis values and ground truth

For E type composite laminate,

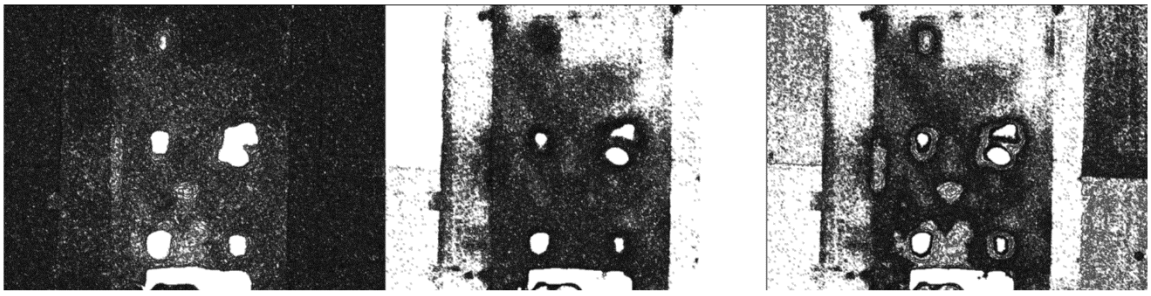

Figure 64: Maximum Probability

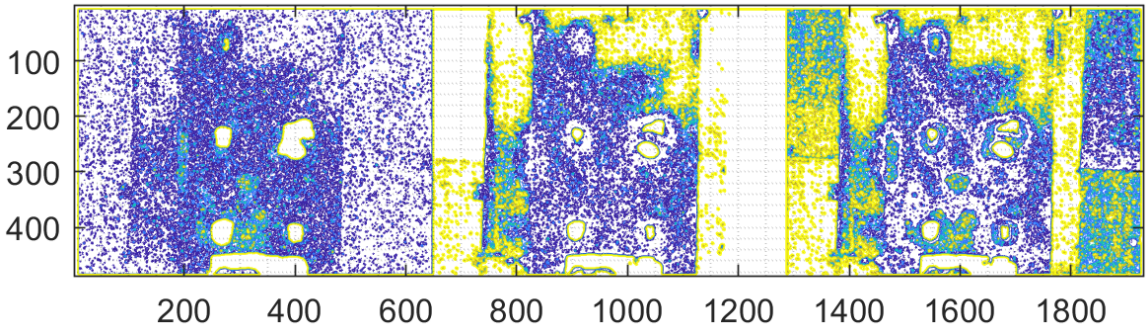

Figure 65: Contour Image for Maximum Probability

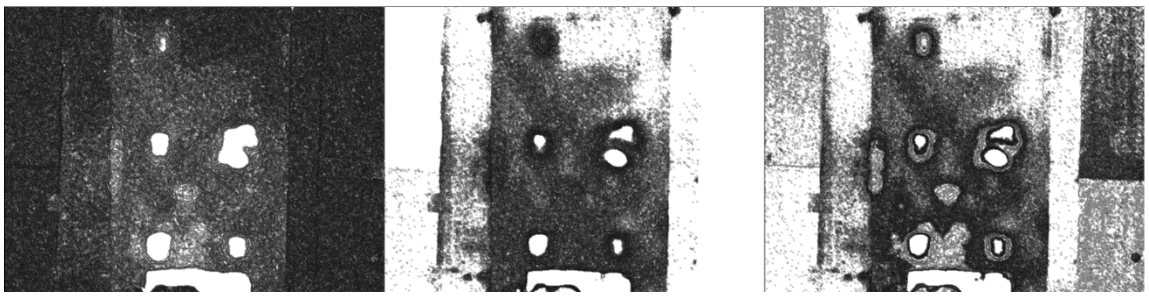

Figure 66: Uniformity of Energy

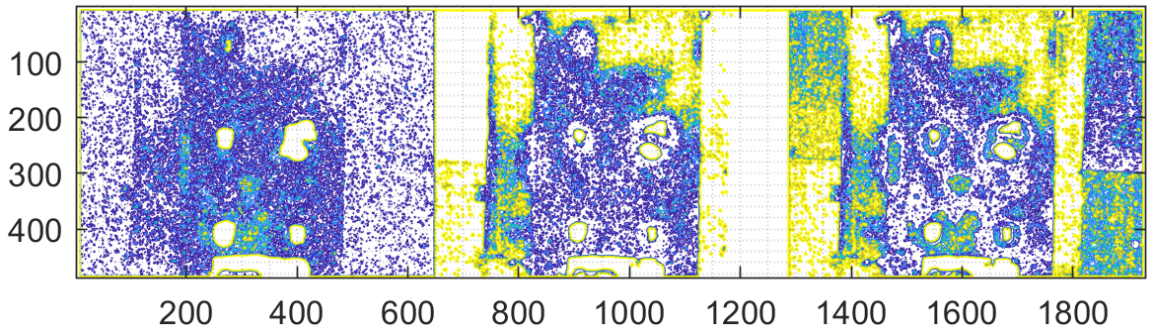

Figure 67: Contour Image for Uniformity of Energy

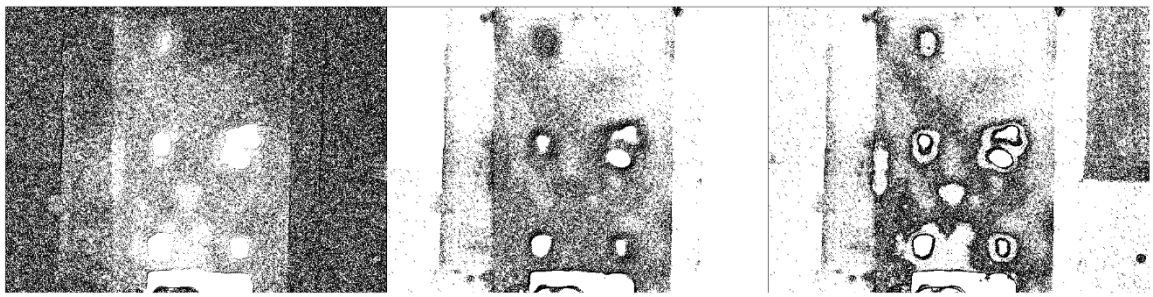

Figure 68: Inverse difference moment of order k

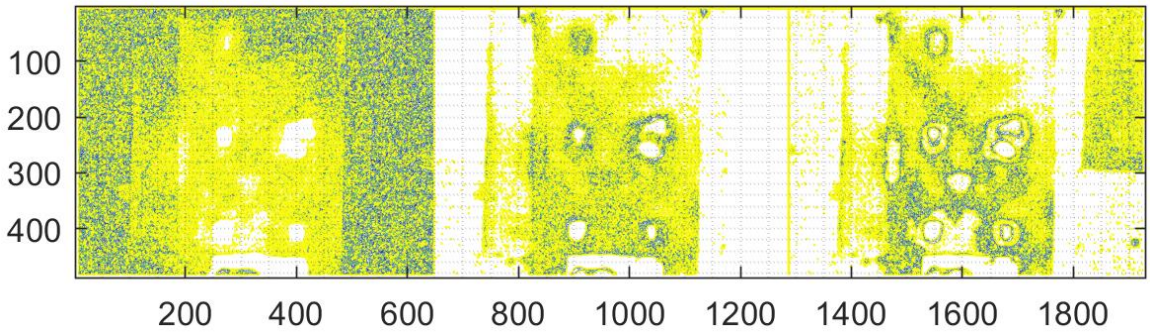

Figure 69: Contour Image for Inverse difference moment of order k

Figure 70: Contrast

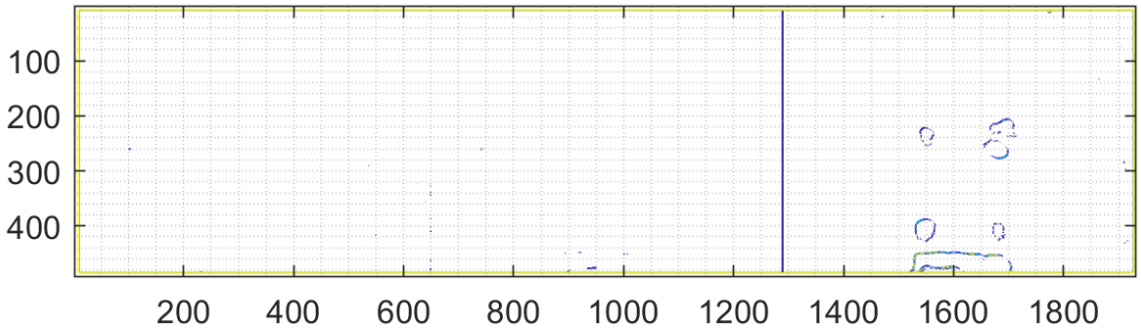

Figure 71: Contour Image for Contrast

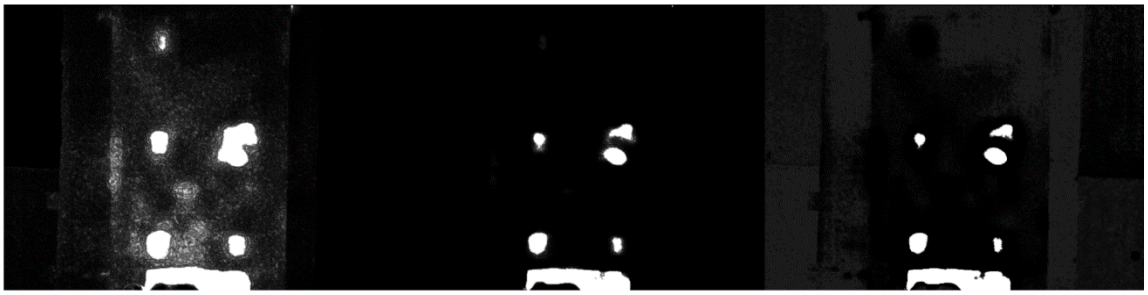

Figure 72: Variance

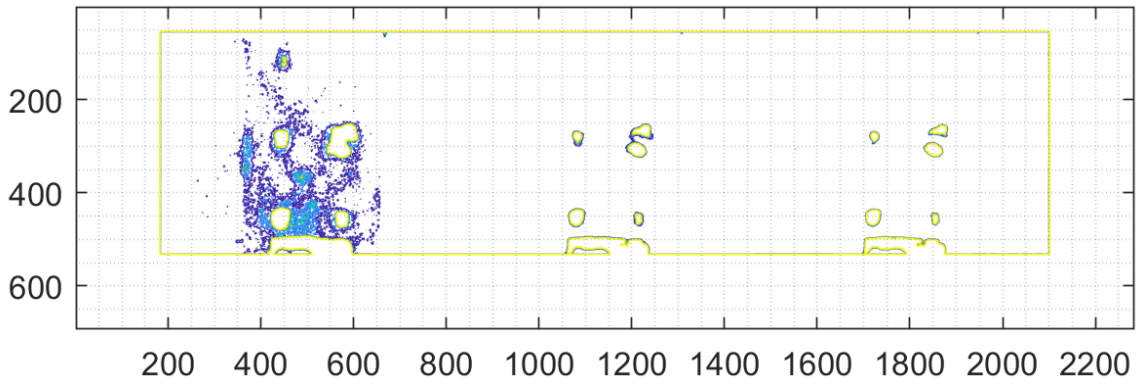

Figure 73: Contour Image for Variance

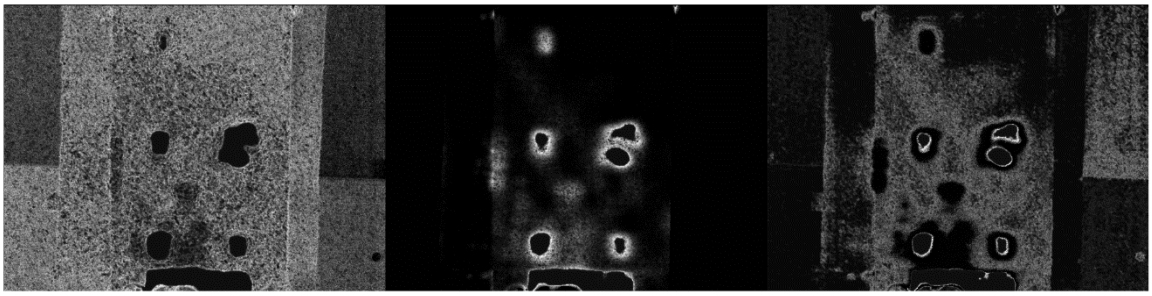

Figure 74: Correlation

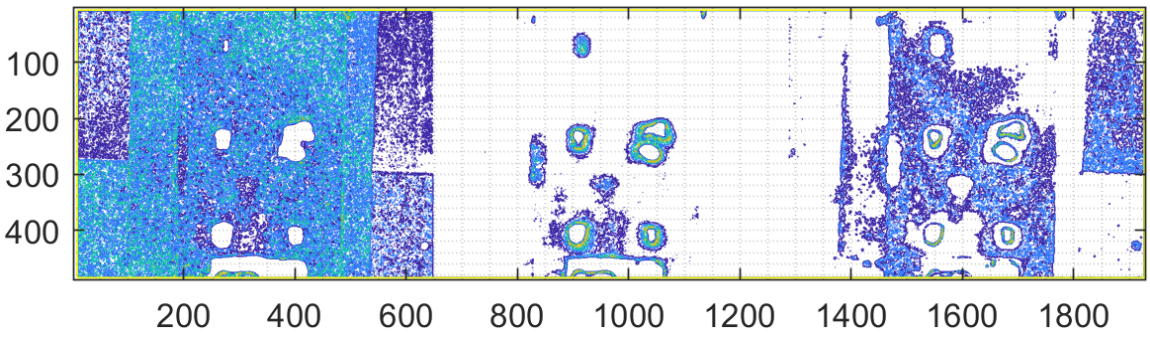

Figure 75: Contour Image for Correlation

As observed from the above images, the correlation textural feature contributes the highest in differentiating the defects in the image.

Dimension	Ground Truth (mm)	Image Analysis Value (mm)	Error %
A	25.4	37.674	48.32
B	50.8	50.232	1.11
C	12.7	-	-
D	25.4	37.674	48.32
E	25.4	37.674	48.32
F	25.4	25.116	1.11
G – 12.7	266.7	219.765	17.6
H – 25.4	152.4	106.743	29.96
I – 6.35	69.85	-	-

Table 13: Comparison of analysis values and ground truth

Below is the comparison of the above discussed image processing methods:

Algorithm/Method	Computation Time (secs)		Average Error %	
	D type	E type	D type	E type
Otsu Method	0.734	3.094	4.99	17.25
Tsai Method	0.372	0.475	9.34	16.10
Niblack Method	1.100	6.089	24.05	17.82
Hamadani Method	2.49	7.49	3.975	19.42
Sapina Method	412.51	397.74	9.08	27.82

Table 14: Comparison of analysis values and ground truth

Note: For Hamadani and Sapina method, the given computation time is calculated for obtaining all the thermal images.

It should be noted that the observations are specific to the test specimen used, the orientation of the composite laminate and experimental environment. One side of the laminates is smooth and the other side is relatively rough. The above observations and calculations are obtained by observing the rough side of the laminates. If the composite laminates are flipped and the complete experimentation is carried out, the obtained images are blurry and distorted due to excess noise in the image. Therefore, for this experimentation the laminates should be installed so that the rough surface is observed through the IR camera.

3.3

DEPTH ESTIMATION

Damages and defects are generally located at a depth from the surface of a component. Determining the depth of the defect is one of the most important aspect of an NDE testing. The above algorithms used for defect detection in the thermal images, the x and y coordinates of the defects in the composite laminate are determined. In this section, an analytical method of determining the depth of the defect is discussed. The temporal plot (temperature-time plot) of the defects is used in this method. The relation between the depth of the defect and time quantities from the temporal plot is studied and used for determining the defect depth.

We define three quantities in the temperature-time curve and its derivatives and map them to the defect depth. The three time quantities are:

1. **Half – maximum power time (t_H):** This is defined as the time at which the temperature-time curve reaches half maximum power i.e. $\frac{1}{\sqrt{2}}$ of the peak temperature of the temporal plot.
2. **Peak slope time (t_P):** This is defined as the time at which the first derivative or the slope of the temperature-time curve reaches the maximum value.
3. **Second derivative peak time (t_S):** This is defined as the time at which the second derivative of the temperature-time curve reaches the maximum value.

The E type composite laminate is analyzed for depth profiling as the defects are located at different depths. 6 defects are present in the composite laminate and the respective half maximum power time, peak slope time and the second derivative peak time are recorded during the experiment are given below:

Defect Depth (mm)	Half Maximum Power Time t_H (sec)	Peak Slope Time t_P (sec)	Second Derivative Peak Time t_S (sec)
0.296	14	11.5	0.997
0.59	14.6329	12.32	1.558
0.88	15	12.08	5.598
1.184	15.52	12.76	6.517
1.482 (circle)	17.0033	14.04	6.477
1.482	17	14.04	7.596

Table 15: Time quantities for defects at different depths

From the previous depth estimation methods for different NDE methods reviewed from the literature review, the time quantities are observed to be directly proportional to the value of depth squared of the defect.

The time quantities are plotted against the value of depth squared and using linear regression analysis the relationship between them is determined.

For the half maximum power time, the linear relation is determined to be

$$\mathbf{t_H = 1.353d^2 + 13.95} \quad (73)$$

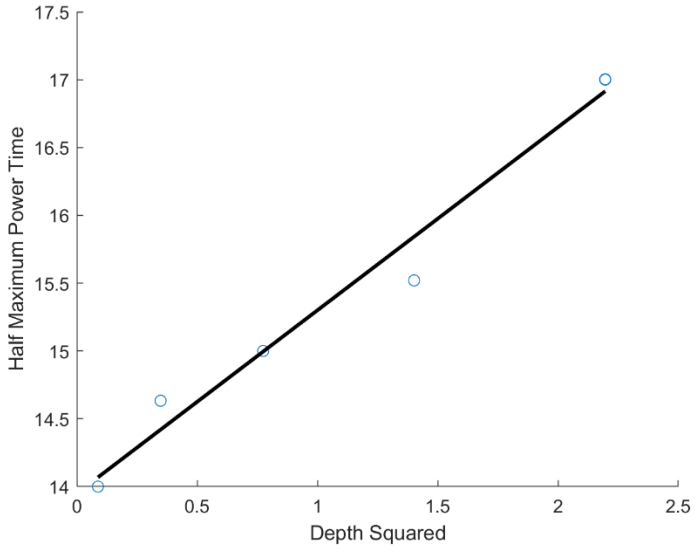

Figure 76: Depth Squared vs Half Maximum Power Time

The R^2 value of the linear regression is 0.978 which indicates a good correlation between the data points and the linear fitting function.

Half Maximum Power Time t_H (sec)	**Theoretical Defect Depth (mm)**	**Experimental Defect Depth (mm)**
14	0.296	0.1922
14.6329	0.59	0.71
15	0.88	0.881
15.52	1.184	1.077
17.0033	1.482 (circle)	1.5095
17	1.482	1.5014

Table 16: Comparison of theoretical and experimental defect depths

For the peak slope time, the linear relation is determined to be

$$\mathbf{t_P = 1.11d^2 + 11.494} \quad (74)$$

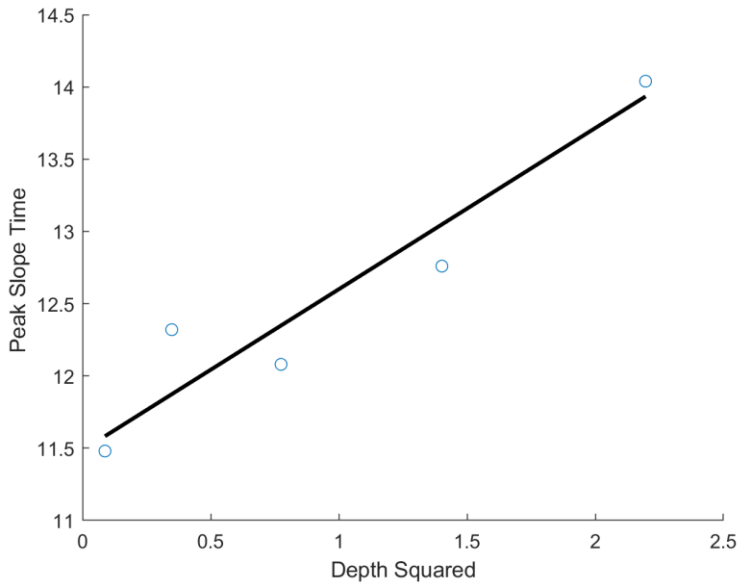

Figure 77: Depth Squared vs Peak Slope Time

The R^2 value of the linear regression is 0.9304 which indicates a good correlation between the data points and the linear fitting function.

Peak Slope Time t_P (sec)	**Theoretical Defect Depth (mm)**	**Experimental Defect Depth (mm)**
11.5	0.296	0.0735
12.32	0.59	0.8625
12.08	0.88	0.7265
12.76	1.184	1.0679
14.04	1.482 (circle)	1.5144
14.04	1.482	1.5144

Table 17: Comparison of theoretical and experimental defect depths

For the second derivative peak time, the linear relation is determined to be

$$t_S = 2.763d^2 + 1.556 \quad (75)$$

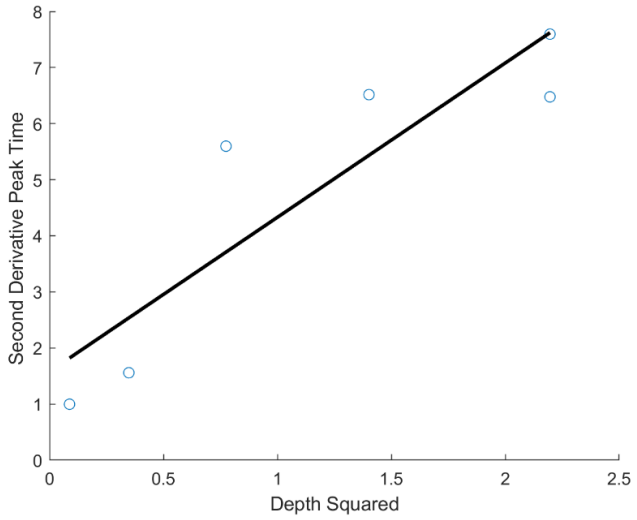

Figure 78: Depth Squared vs Second Derivative Peak Time

The R^2 value of the linear regression is 0.8074 which indicates a good correlation between the data points and the linear fitting function.

Second Derivative Peak Time t_S (sec)	**Theoretical Defect Depth (mm)**	**Experimental Defect Depth (mm)**
0.99	0.296	-
1.558	0.59	0.0269
5.598	0.88	1.2095
6.517	1.184	1.3399
6.477	1.482 (circle)	1.3345
7.596	1.482	1.4785

Table 18: Comparison of theoretical and experimental defect depths

CHAPTER 4
PROCESS PARAMETER STUDY

Parameters of an experiment are defined as the characteristics or the factors of an experiment which affects its output or the efficiency of the output. For this experiment, there are 3 parameters which can be numerically defined, and we intend to investigate its effect on the output. The parameters are defined below:

1) Number of pulses

   The number of ultrasonic pulses which are applied to the specimen in given time.

2) Pulse Duration (ms)

   Pulse duration is defined as the time duration for which the ultrasonic signal is applied to the specimen.

3) Time Duration between Pulses (ms)

   This is defined as the time delay between two consecutive pulses applied to the specimen.

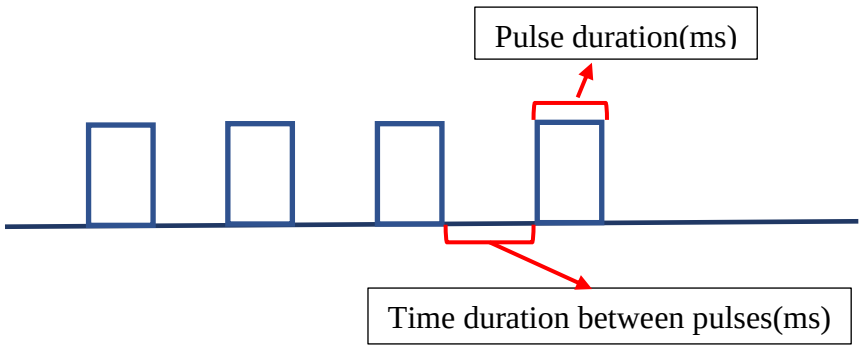

Figure 79: Graphical representation of the ultrasonic pulse signal

From chapter 3.2, it can be observed that the Hamadani method for image analysis is the most accurate for detecting and locating the defects in the composite laminate. Hamadani method is used for comparing the results for different process parameters. The value of k_1 and k_2 is selected as 1.5 for accuracy. The dimension of the square defect with 1'' side length will be anlayzed for different values of the process parameters.

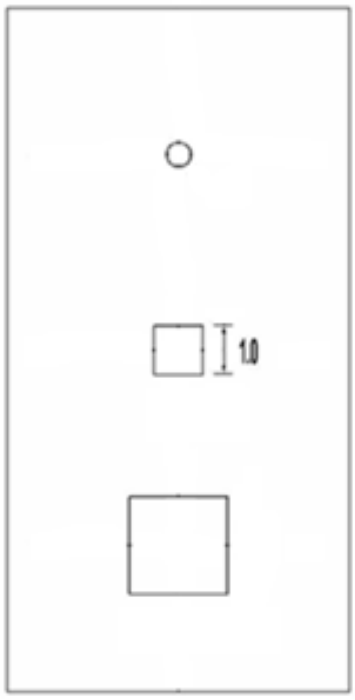

Figure 80: Ground Truth Dimension

Also, the effects of process parameters on the probability of detection of the defects present in the D type composite is also analyzed and discussed.

1. Number of Pulses

For analyzing the effect of the number of ultrasonic pulses during the experiment on the temperature increase, we will set the following parameters as given below:

Pulse duration: 200ms

Time delay between the pulses: 250ms

For this study, the effect of these parameters on the detection of defects in the D type composite laminate and the probability of detection of these defects is analyzed and compared.

The following data was recorded for the experiment:

No. of Pulses	Pulse Duration (ms)	Time Delay between Pulses (ms)
10	200	250
15	200	250
20	200	250
25	200	250
30	200	250
40	200	250

Table 19: Process Parameters Values for Number of Pulses

Ground Truth	Number of Pulses	Image analysis value	Error %
25.4 mm	10	21.976 mm	13.48
	15	25.116 mm	1.11
	20	28.255 mm	11.24
	25	31.395 mm	23.6
	30	31.395 mm	23.6
	40	-	-

Table 20: Comparison of dimension error for different number of pulses

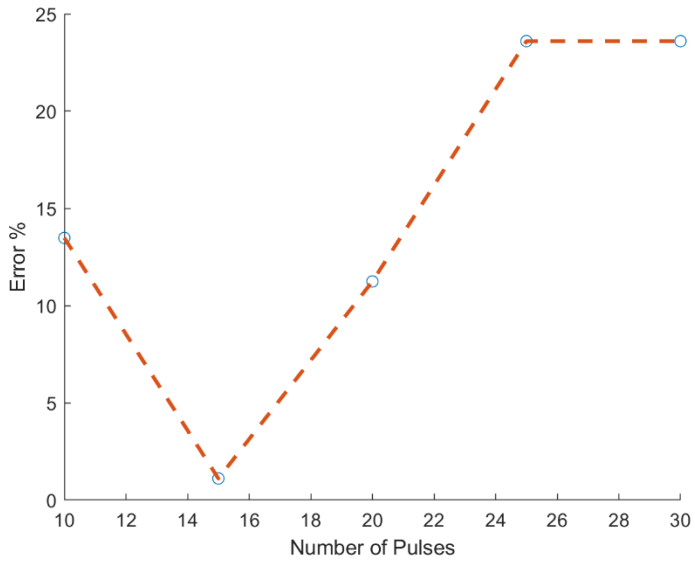

Figure 81: Number of pulses vs Error %

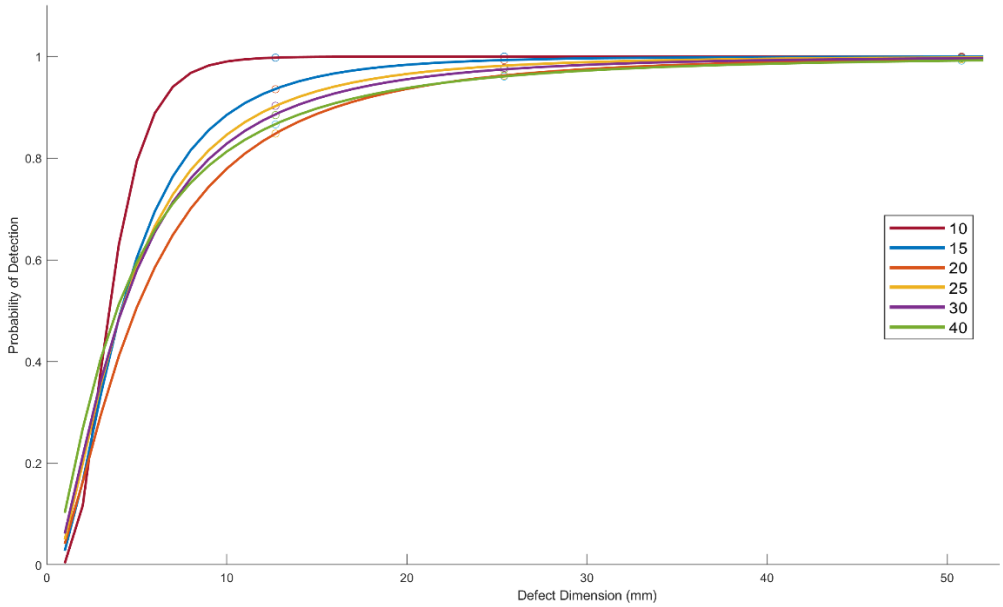

Figure 82: POD Curves for different number of pulses

2. Pulse Duration

For analyzing the effect of the pulse duration during the experiment on the temperature increase, we will set the following parameters as given below:

No. of Pulses: 10

Time delay between the pulses: 300ms

Note: The time delay between the pulses should always be greater than the value of pulse duration.

The following data was recorded for the experiment:

Pulse Duration (ms)	No. of Pulses	Time Delay between Pulses (ms)
230	10	300
240	10	300
250	10	300
260	10	300
270	10	300
280	10	300

Table 21: Process parameters values for pulse duration

Ground Truth	Pulse Duration	Image analysis value	Error %
25.4 mm	230ms	25.116 mm	1.11
	240ms	25.116 mm	1.11
	250ms	25.116 mm	1.11
	260ms	25.116 mm	1.11
	270ms	25.116 mm	1.11
	280ms	25.116 mm	1.11

Table 22: Comparison of error for different pulse durations

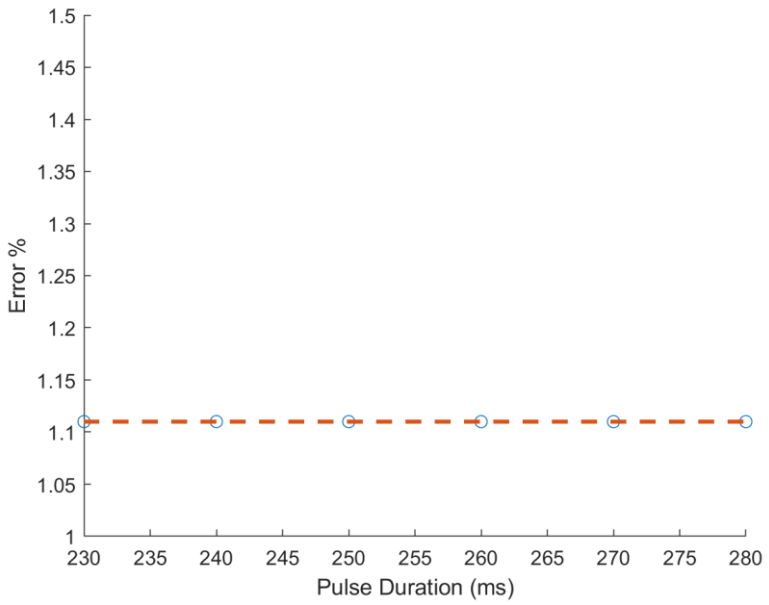

Figure 83: Pulse Duration vs Error %

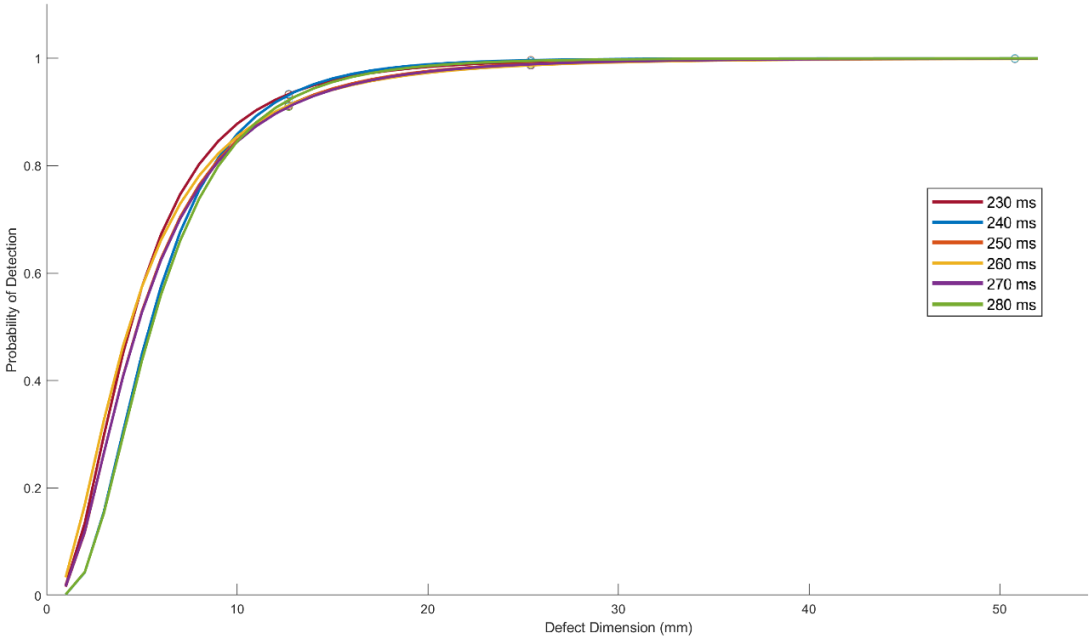

Figure 84: POD Curves for different pulse durations

3. Time delay between Pulses

For analyzing the effect of the time delay between two consecutive pulses during the experiment on the temperature increase, we will set the following parameters as given below:

No. of Pulses: 10

Pulse Duration: 200ms

The following data was recorded for the experiment:

Time Delay between Pulses (ms)	No. of Pulses	Pulse Duration (ms)
300	10	200
310	10	200
320	10	200
330	10	200
340	10	200
350	10	200

Table 23: Process parameters values for time delay between pulses

Ground Truth	Time delay between pulses	Image analysis value	Error %
25.4 mm	300ms	21.976 mm	13.48
	310ms	23.86 mm	6.06
	320ms	21.976 mm	13.48
	330ms	21.976 mm	13.48
	340ms	20.093 mm	20.89
	350ms	20.72 mm	18.42

Table 24: Comparison of error for different time delay between pulses

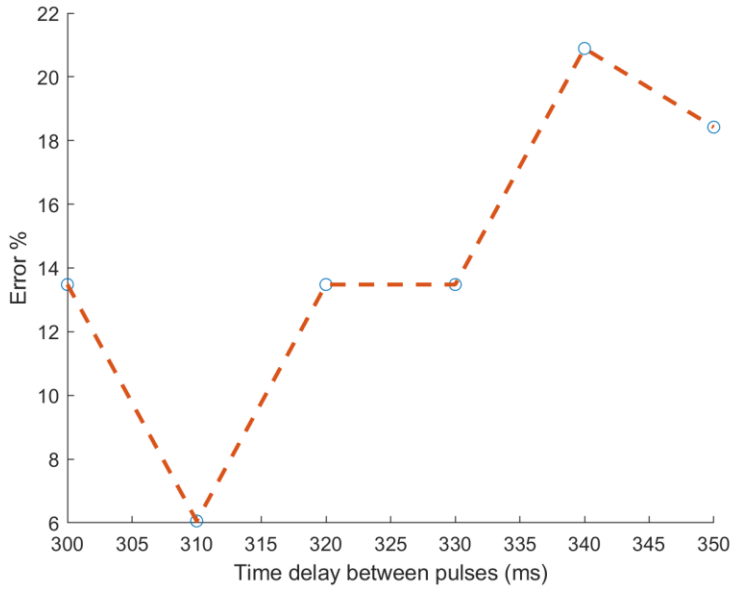

Figure 85: Time delay between pulses vs Error %

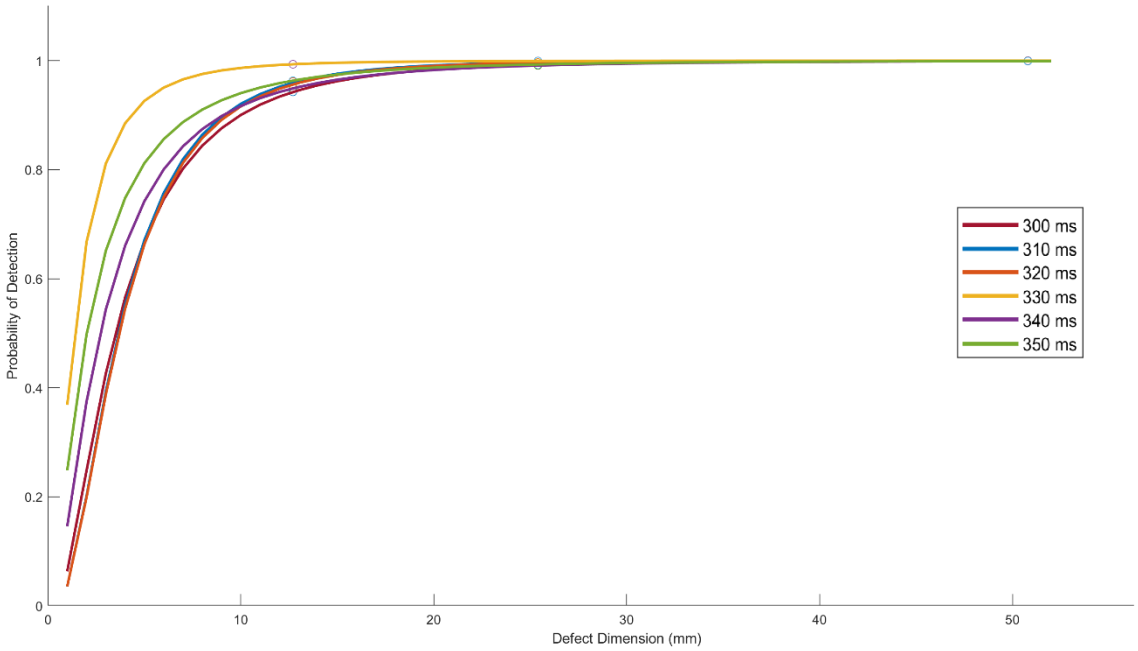

Figure 86: POD Curves for different time delays between pulses

4.1

DISCUSSION

a) Number of pulses (N)

For the percentage error in the dimension of the defect, as the trend of the graph in figure 81 indicates, as the number of pulses applied increases, the error percentage of the dimension first decreases then increases as the number of pulses increases. It can be observed that the trend of the graph is not monotonic. This is because initially when the number of pulses reaches 15 from 10, due to higher pulses applied in a period of time, the temperature increase is higher resulting in a more accurate than for 10 pulses. As the number of pulses increase, the energy absorbed by the composite laminate increases. This energy is also absorbed by the impurities and discontinuities formed during the manufacturing process of the composite laminate resulting in temperature increase in other areas of the composite laminate other than the defect areas. Also due to thermal diffusion effect between the defect and non-defect area, the error percentage of dimension increases with increasing pulses. After a certain number of pulses, the temperature variation throughout the composite laminate remains approximately the same as it can be observed from the graph.

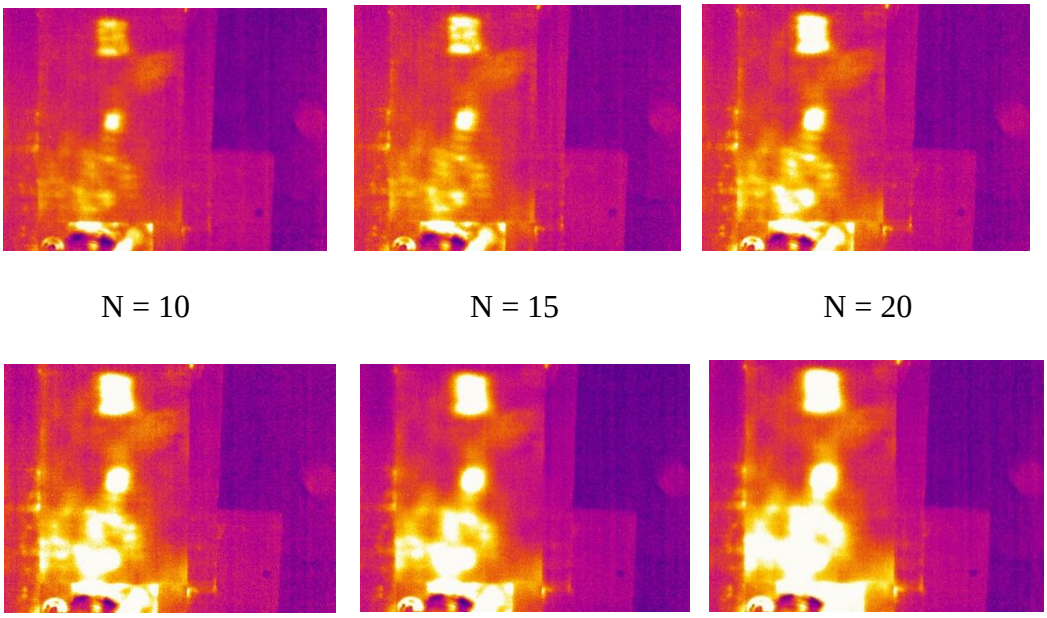

Figure 87: Thermal images for increasing number of pulses

For the probability of detection, it can be observed from the POD curves that for the defects with diameter 0.5'' and side length 1" the POD decreases with increasing the number of pulses. Whereas for the defect with side length 2", the POD remains unaffected by the number of pulses applied to the specimen.

b) Pulse Duration

For the percentage error in the dimension of the defect, as the trend of the graph in figure 83 indicates, as the duration for which the ultrasonic pulse is applied increases, the accuracy of detection remains unaffected as the pulse duration increases.

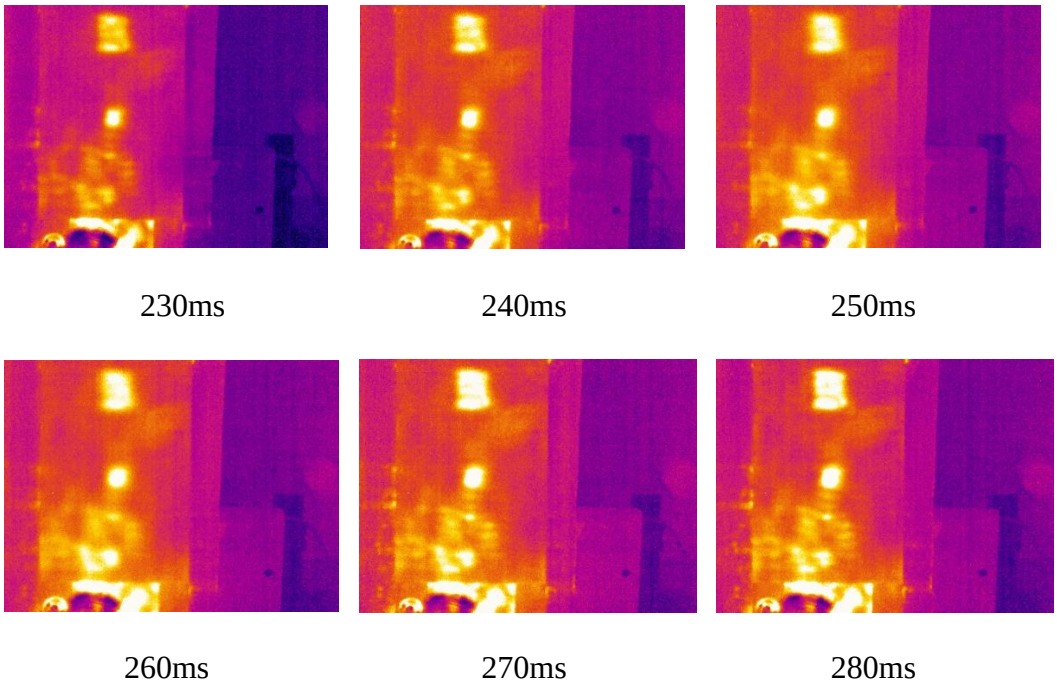

Figure 88: Thermal images for increasing pulse duration

For the probability of detection, it can be observed from the POD curves that for the defects with diameter 0.5'' the POD decreases with increasing the pulse duration. Whereas for the square defects with side length 1" and 2", the POD is approximately the same and remains unaffected by the duration of pulse applied to the specimen.

c) Time delay between pulses

For the percentage error in the dimension of the defect, as the trend of the graph in figure 85 indicates, as the time delay between pulses increases the error percentage of defect detection does not follow a trend. The mean error is 14.3 % and standard deviation of 4.66. This indicates that the increase in time delay between pulses does not have a substantial effect on the average error percentage of dimension.

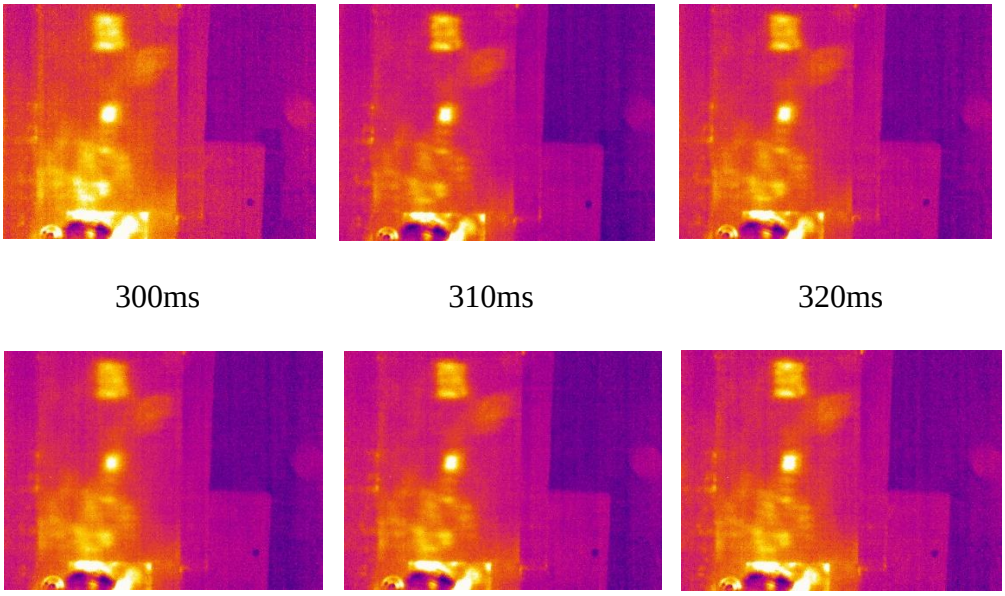

Figure 89: Thermal images for increasing time delay between pulses

For the probability of detection, it can be observed from the POD curves that for all the defects is approximately equal except for the case when the time delay between two consecutive pulses is 330ms.

Analyzing all the process parameters, the optimum result is achieved for the following values of the process parameters:

1) Number of Pulses: 10
2) Pulse Duration: 230ms – 260ms
3) Time delay between pulses: 330ms

CHAPTER 5

CONCLUSION

Using SONIC IR NDT enables the detection of subsurface defects present in the composite laminates using infrared cameras. Through the experimentation, it can be concluded that the SONIC IR NDT method is quick, has relatively easier setup and gives accurate results. The primary objective of this research is to use SONIC IR to detect the location and depth of subsurface defects in the composite laminate through the investigation of existing image processing and analysis algorithms. The algorithms are compared based on computation time and accuracy with respect to the defect location and dimension. Observing the results for all the image processing algorithms, the most accurate and quick results are obtained using Hamadani method (dedicated algorithm) with an average accuracy of 3.975 % for D type composite laminate and 19.42 % for E type composite laminate. It should be noted that none of the algorithms discussed were able to detect the circular defect of diameter 0.5'' in both D and E type of composite laminate. The depth of the defects is estimated using time quantities from the temporal history of the defects through linear regression. Half maximum power time gives the most accurate results as compared to peak slope and second derivative peak time. Probability of detection is observed to increase with increasing defect side length and decreases as the defect depth increases.

Lastly, the effect of the three process parameters namely number of pulses applied, pulse duration and time delay between consecutive pulses on the defect detection accuracy and probability of detection is analyzed and discussed.

CHAPTER 6

FUTURE WORK

1. Use of inverse heat conduction framework for 3D reconstruction of the damages in the composite laminate. This method provides a more accurate representation of the defect delaminations in the specimen.
2. Further investigation on two-dimensional probability of detection (POD) for defects considering the length and depth of the defects resulting into a more accurate POD analysis.
3. Using Green's function procedure to derive the relationship between the temperature profile and the input parameters of the experiment to obtain a theoretical model and compare it with the linear regression models for depth estimation of the defects.
4. Investigating more process parameters, for example, the frequency of ultrasonic pulse, orientation of the composite laminate on the defect detection and the probability of detection of defects thereby increasing the accuracy of the NDT method.

REFERENCES

[1] Francesco Ciampa, Pooya Mahmoodi, Fulvio Pinto, Michele Meo, Recent Advances in Active Infrared Thermography for Non-Destructive Testing of Aerospace Components, Sensors, 2018

[2] Xiaoyan Han, L D Favro, R L Thomas, Sonic IR Imaging of delaminations and disbonds in composites, Journal of Physics D: Applied Physics 44,2011

[3] X. Han, S. Zhao, D. Zhang, A. Lubowicki, L. Favro, R. Thomas, G. Newaz, Develop Sonic Infrared Imaging NDE for Quantitative Assessment on Damage in Aircraft Composite Structures, 11th International Conference on Quantitative InfraRed Thermography, 2012

[4] Rudi Heriansyah, S.A.R. Abu-Bakar, Defect detection in thermal image for nondestructive evaluation of petrochemical equipments, NDT and E International 42, 2009

[5] Mehmet Sezgin, Bulent Sankur, Survey over image thresholding techniques and quantitative performance evaluation, Journal of Electronic Imaging 13, 2004.

[6] Nobuyuki Otsu, A Threshold Selection Method from Gray-Level Histograms, IEEE Transactions on Systems, Man, and Cybernetics 9,1979

[7] Azriel Rosenfield, Pilar De La Torre, Histogram Concavity Analysis as an Aid in Threshold Selection, IEEE Transactions on Systems, Man, And Cybernetics 13, 1983

[8] J. N. Kapur, P. K. Sahoo, A. K. C. Wong, A New Method for Gray-Level Picture Thresholding Using the Entropy of the Histogram, Computer Vision, Graphics, and Image Processing 29, 1985

[9] Wen-Hsiang Tsai, Moment-Preserving Thresholding: A New Approach, Computer Vision. Graphics, and Image Processing 29, 1985

[10] Lalit Prakash Saxena, Niblack's binarization method and its modifications to real-time applications: a review, Artif Intell Rev, 2019

[11] Rozalija Sapina, Computing Textural Features Based on Co-occurrence Matrix for Infrared Images, IEEE, 2002

[12] X. Maldague , J.C. Krapez , D. Poussart, Thermographic nondestructive evaluation (NDE): an algorithm for automatic defect extraction in infrared images, IEEE Transactions on Systems, Man, and Cybernetics 20, 1990

[13] Jean Christophe Olivo, Automatic Threshold Selection using the Wavelet Transform, Graphical Models and Image Processing 56, 1994

[14] Peyman Hedayati Vahid, Automatic Defect Detection and Depth Estimation using Pulsed Thermography,2014

[15] J. G. Sun, Analysis of Pulsed Thermography Methods for Defect Depth Prediction, Journal of Heat Transfer 128,2006

[16] Omar Obeidat, Qiuye Yu, Xiaoyan Han, Profiling defect depth in composite materials using thermal imaging NDE,NDT and E International 100 , 2018

[17] Jun-zhen Zhu, Chao-sheng Zhang, Fu-zhou Feng, Qing-xu Min, Chao Xu, Study on probability of detection for fatigue cracks in sonic infrared imaging, Infrared Physics & Technology 77, 2016

[18] N Yusa, Probability of detection model for the non-destructive inspection of steam generator tubes of PWRs, IOP Conf. Series: Journal of Physics: Conf. Series 860, 2017

[19] D Kanzler, C Müller and J Pitkänen, Probability of detection for surface breaking holes with low-frequency eddy current testing – a non-linear multi-parametric approach, ECT POD, 2019

[20] Vamsi Krishna Rentala, Phani Mylavarapu, Jai Prakash Gautam, Issues in estimating probability of detection of NDT techniques – A model assisted approach, Ultrasonics 87, 2018

[21] J. DiMambro, D.M. Ashbaugh, C.L. Nelson, and F.W. Spencer, Sonic Infrared (IR) Imaging and Fluorescent Penetrant Inspection Probability of Detection (POD) Comparison, AIP Conference Proceedings 894, 2007

[22] Zhi Zeng,Ning Tao,Lichun Feng, Cunlin Zhang, Specified value based defect depth prediction using pulsed thermography, Journal of Applied Physics 112, 2012

APPENDIX A

COMPOSITE LAMINATE SPECIFICATIONS

For this study, two types of composite laminates with pre-inserted delaminations at different depths are used. The details of the composite laminates and the delamination defects are given below:

Uni-directional carbon: Toray, T700G-12K-31E/#3900

Epoxy-glass tabs: 1/8 inch or 1/16-inch FR-4 e-glass pressed laminate at the gripping area

Adhesive: Hysol EA9360

Size: 7'' x 14''

The composite laminate specifications are given below:

Layup		No. of Layers	Delamination
$[90_2/+45_2/-45_2]$ s	D	12	Inserted Teflon delaminations at the middle layer
$[90_2/+45_2/-45_2]$ s	E	12	Inserted Teflon delaminations between layers

Table A.1: Composite Laminate Specifications

Layup: D

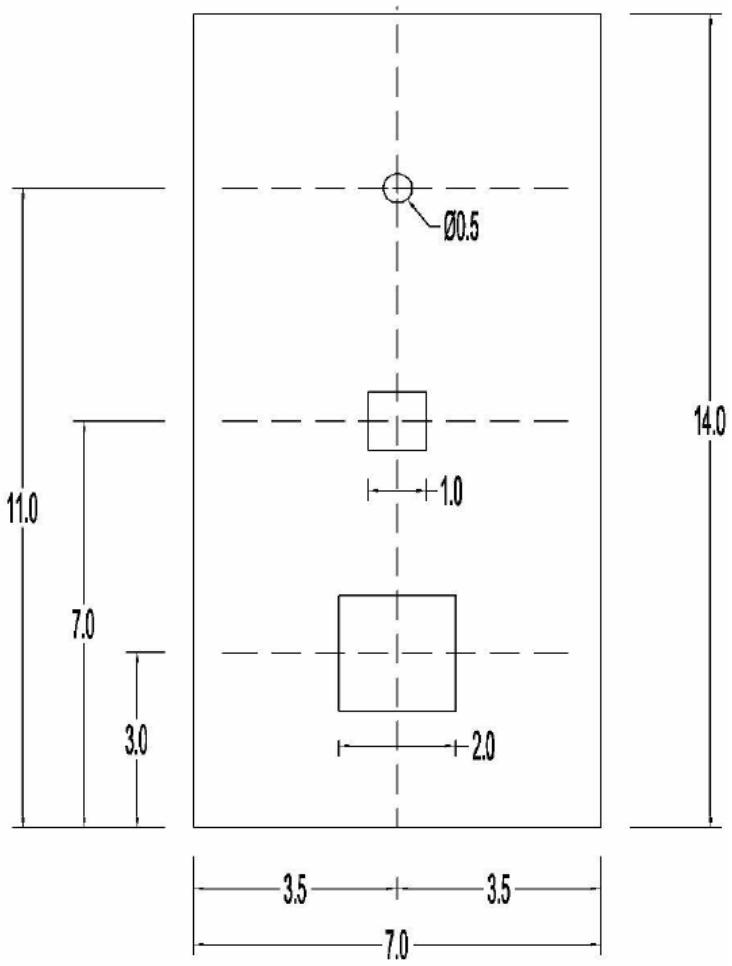

Figure A.1: Delamination inserted at middle layer for layup D (unit: inch)

Layup: E

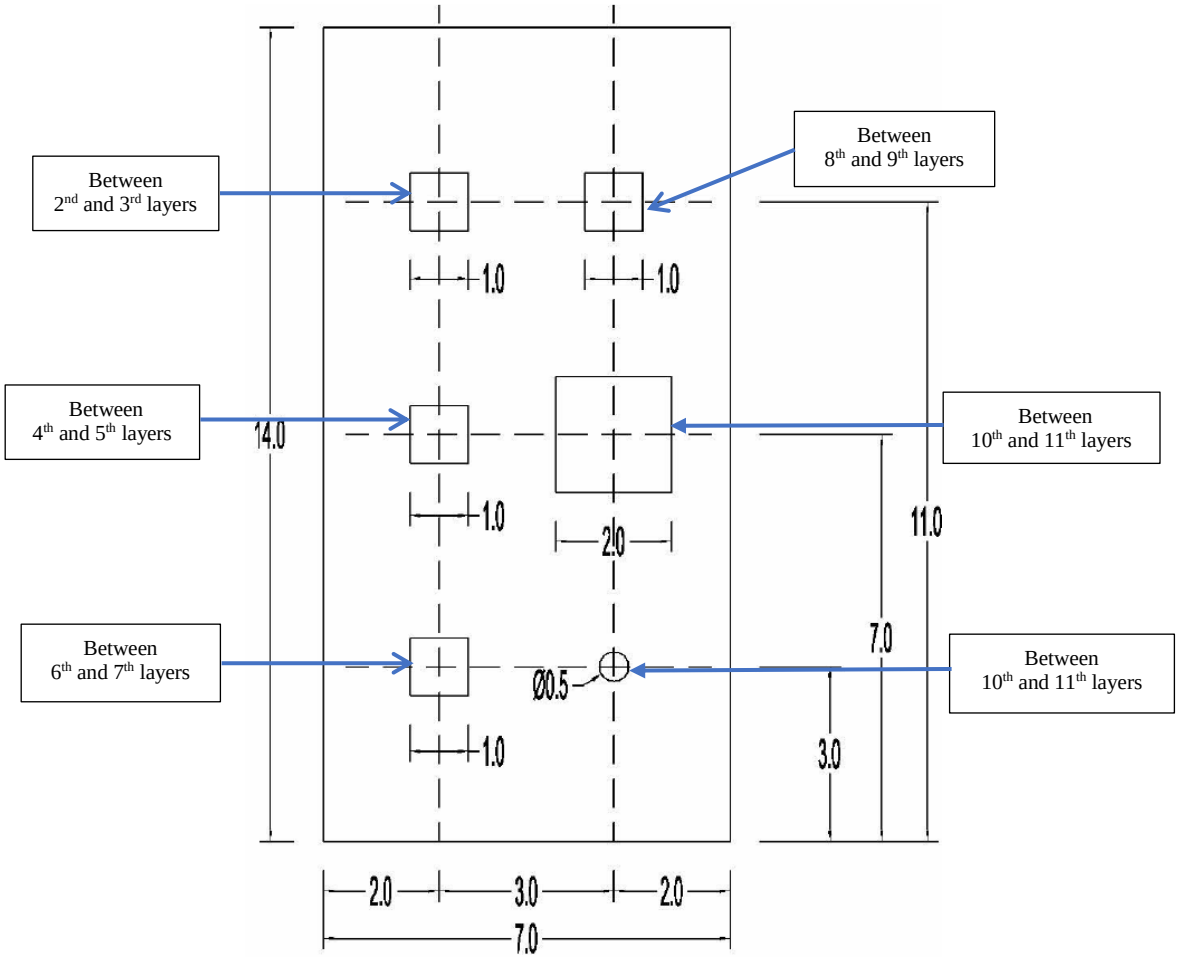

Figure A.2: Delamination inserted between different layers (unit: inch)

The composite laminate has 12 layers. The Figure A.2 illustrates the location and depth of the defects in the composite laminate.